2D Geometric Morphometrics of Murine Mandibular Toothrows from Liang Bua (Flores, Indonesia): Implications for Taxonomic Identification

Anneliese Eber

A thesis presented to Lakehead University

in partial fulfillment of the requirements of

Master of Science in Archaeological Science

Thunder Bay, Ontario, Canada, 2022

Table of contents

Acknowledgements

First, I would like to thank Drs. Matt Tocheri, E. Grace Veatch, and Timothy Kaiser for all your time, effort, and support during this process.

Dr. Tocheri, thank you for everything you have done to make this project possible. Thank you for pushing me to expand my knowledge, research skills, and critical thinking ability. Your support, guidance, and encouragement has been invaluable to my research, I would not have made it here without you. Dr. Veatch, thank you for all your assistance collecting and photographing teeth for me; without your help, I would not have been able to complete this project during a pandemic. Thank you for sharing all your knowledge about the Liang Bua rats and always being there to guide me and give me helpful advice and encouragement. Dr. Kaiser, thank you for your thoughtful and kind comments about my research, your guidance throughout my time at Lakehead has been invaluable. Thank you to my external examiner, Dr. Lucas Delezene, for taking the time to read my thesis and provide me with comments.

I would also like to thank Lakehead's Anthropology Department. Thank you to Jennifer McKee for always being just an email away and always being willing to help me and answer questions. Thank you to all my instructors throughout the last two years, Drs. Scott Hamilton, Jessica Metcalfe, Matt Tocheri, and Adam Cornwell. I am grateful to have had the opportunity to learn from all of you. Thank you to everyone in the Human Origins and Primate Evolution Laboratory who attend the weekly meetings and share their work, even on holidays. I have learned so much listening to the many different research projects. Thank you to my fellow MSc Archaeological science cohort members, Agus Julianto, Nico Alamsyah, Shane Teesdale, and Nick Kuncewicz, it has been great getting to work and learn with all of you. Thank you

Lastly, I would like to thank all my family for listening to all my rat-related rants over the last few years. Thank you to my siblings Lukas and Gabrielle for always being willing to listen to my research and give helpful advice. Thank you to my parents Michelle and Herwig for your unconditional support while I pursued my dreams. A special thank you to Randy Williamson for your unwavering support the last two years while I spent endless hours working and researching.

List of tables

List of figures

Abstract

This study uses—and evaluates the efficacy of—two-dimensional geometric morphometrics (2DGM) to quantitatively characterize the size and shape of murine rodent (i.e., rat) mandibular molar rows from the archaeological site of Liang Bua, a limestone cave located on the Indonesian island of Flores and the type site of *Homo floresiensis*. Murine remains make up a significant portion of Liang Bua's sizable faunal assemblage and contribute significantly to understanding the paleoecology of western Flores. As such, it is essential to develop robust methodologies to accurately assess the taxonomy of these remains. Using images of complete mandibular toothrows, this study aims to test the functionality of 2DGM for taxonomic assessments based on the size and shape variation present in the Liang Bua murine assemblage. The results show that 2DGM offers important information about mandibular toothrow size and shape that can be used in conjunction with qualitative and other quantitative data for murine species identification at Liang Bua and other archaeological sites on Flores. Additionally, this study explores the effects of image angle and tooth wear on 2DGM analyses and provides several recommendations for how to mitigate these potential issues in future work. Since the Liang Bua murine remains represent multiple species of varying body sizes and habitat preferences, quantitative variation and descriptions of previously uncharacterized inter- and intra-species variation described in this study will help to facilitate ongoing paleoecological reconstructions of the cave's history.

Introduction

      Teeth are integral to mammalian taxonomy because they contain critical information that is used to define and differentiate species (Swindler, 2002; Bailey, 2004; Hillson, 2005). While many vertebrates (e.g., reptiles and fish) are polyphyodont (i.e., teeth are constantly replaced throughout life), mammals are different in that they only have two sets of teeth (diphyodont) (Buchtová et al., 2012). Mammals develop deciduous teeth first (sometimes referred to as milk or baby teeth), which then fall out later during development and are replaced with larger, permanent teeth (Ungar, 2014). Furthermore, mammals are heterodont, meaning that they have different kinds of teeth. The anterior dentition includes incisors and canines, both of which have a single cusp; in contrast, the post-canine dentition consists of premolars and molars, both of which are typically multi-cusped (Ungar, 2014). Multiple cusps result in more complex crown and root morphology and as a result, analyses of post-canine teeth, particularly molars, dominate the literature (Wood and Abbott, 1983; Wood et al., 1983; Calede and Hopkins, 2011; Gómez-Robles et al., 2015; Calede and Glusman, 2017; Hulme-Beaman et al., 2018a, b). The presence or absence of each tooth type (e.g., not all mammals have canines) and how many of each tooth type (e.g., three versus four premolars) varies among mammalian taxa (Ungar, 2014). This variation is documented using the dental formula (Ungar, 2014), which summarizes the number of each tooth type in a particular quadrant (e.g., upper left jaw) of the dentition (Hillson, 2005). For example, rats have a typical dental formula of 1:0:0:3 indicating that each quadrant has one incisor, no canine, no premolars, and three molars, resulting in a total of 16 permanent teeth (Misonne, 1969). This differs from *Homo sapiens* which has an adult dental formula of 2:1:2:3 for both the upper and lower jaws, indicating that each quadrant typically has two incisors, one canine, two premolars, and three molars (Ungar, 2014), resulting in a total of 32

permanent teeth (Hillson, 1996, 2005; Ungar, 2014). Major differences in dental formula are often taxonomically diagnostic, particularly in primates (Hillson, 2005). Additionally, there is considerable variation in tooth size and shape that can be used to inform about mammalian taxonomy, phylogeny, and diet.

Mammalian teeth consist of two parts, the crown and root. The root anchors the tooth into the bony sockets of the mouth and the number of roots for each tooth varies based on the type of tooth (Hillson, 2005). Canines and incisors have single roots and molars have multiple roots, whereas premolars may be single or multi-rooted (Hillson, 2005; Ungar, 2014). Roots are made up of dental pulp, dentin, and cementum (Hillson, 1996, 2005). The innermost layer of the tooth, the pulp chamber, contains the dental pulp and the root canal of the tooth (Hillson, 1996). This is then covered by a layer of dentin, which is enclosed by a layer of cementum rather than enamel (Hillson, 1996). In contrast, the crown is made of enamel (Hillson, 2005), which protects teeth from taphonomic processes (Hillson, 1996) because of its extreme hardness and unique structure (Diekwisch et al., 2002). For this reason, tooth crowns preserve well in the archaeological and fossil records (Hillson, 2005; Ungar, 2014). It is therefore not surprising that teeth are a primary tool for identifying species in archaeological and paleontological assemblages (Bailey, 2004; Gómez-Robles et al., 2008, 2015; Martinón-Torres et al., 2008; Brown and Maeda, 2009; Feranec et al., 2010; McGuire, 2011; Grine et al., 2012; Locatelli et al., 2012, 2015; Delgado et al., 2014; Kaifu et al., 2015).

Although mammalian teeth share an overall similar structure and are composed of the same tissues, the patterns seen in their chewing, or occlusal, surfaces vary greatly, especially within murines (i.e., rat). Since these surface differences are quite distinctive, these features have been used in combination with absolute tooth dimensions to confidently identify specimens to

the genus, if not species, level (Misonne, 1969). While the overall molar structure is typically similar between murine genera, the size, shape, and position of these elements can differ considerably with occlusal cusp patterns ranging from simple to very complex (Misonne, 1969; Musser, 1981). These cusp patterns are formed by the relationship between the individual dental elements (i.e., cusps and auxiliary cusplets) and are influenced by factors such as evolutionary forces and diet (Misonne, 1969; Musser et al., 1981). Even without size, cusp patterns and the unique relationships between dental elements can sometimes be distinctive enough to identify murine genera (Musser, 1981). Moreover, the rat dental formula (one incisor and three molars (Misonne, 1969)) makes murine molars integral for taxonomic identification. However, despite the usefulness of these qualitative characteristics captured in the occlusal patterns and dental formulae of rat dentitions, quantitative measurements can also contribute to confidently identify taxa.

Teeth are measured in a variety of different ways. Traditional measurements record the maximum linear dimensions (length, width, and height) of the tooth crown (Musser, 1981; Hillson, 1996) with the maximum lengths and widths measured mesiodistally and buccolingually, respectively (Hillson, 1996). Such measurements capture the overall size of the tooth and basic aspects of its shape, both of which are useful for documenting variation among individuals, populations, and species (Hillson, 1996, 2005). In recent years, more sophisticated methods for quantifying shape have been developed (Adams et al., 2004, 2013). One of these, geometric morphometrics (GM), stems from traditional measurement theory and has grown into a variety of techniques that provide considerable advantages for studies of shape (Zelditch et al., 2004, 2012). Multiple studies have demonstrated the efficacy of GM for quantifying and visualizing shape variation in many different mammalian taxa (Martinón-Torres et al., 2008;

Gómez-Robles et al., 2007, 2008, 2011, 2015; Skinner et al., 2008; Cucchi et al., 2011; McGuire, 2011; Hulme-Beaman, 2014; Calede and Glusman, 2017; Hulme-Beaman et al., 2018a, b). Due to the ability to quantitatively characterize complex shapes (Cooke and Terhune, 2015), GM has become a standard methodology for answering and exploring questions related to vertebrate phylogeny, taxonomy, functional morphology, and even domestication (Martinón-Torres et al., 2006; Gómez-Robles et al., 2007, 2008, 2011, 2015; Cucchi et al., 2011; McGuire, 2011; Hulme-Beaman, 2014; Calede and Glusman, 2017; Hulme-Beaman et al., 2018a, b; Nozaki et al., 2021). Specific GM techniques are conducted either in two (2DGM) or three dimensions (3DGM). In both 2DGM and 3DGM, data are typically collected as landmarks and/or semilandmarks, which are coordinates (x, y and x, y, z, respectively) that represent homologous[1] or at least reasonably comparable locations on the sampled specimens (Cooke and Terhune, 2015).

Although the process of collecting landmarks differs between 2DGM and 3DGM, the subsequent analytical procedures are relatively similar to one another. Once the landmarks are collected, generalized Procrustes analysis is used to transform and superimpose the landmark data such that only shape data remains (Zelditch et al., 2004, 2012; Cooke and Terhune, 2015). For example, transformation and superimposition remove information about the size, position, and rotation of each specimen (Zelditch et al., 2004, 2012; Cooke and Terhune, 2015). To remove size information, the centroid size[2] is calculated for each specimen by finding the square root of the sum of squared distances of all the landmarks from the average x, y or x, y, z coordinates of all the landmarks (Klingenberg, 2016) and subsequently all specimens are then scaled to a common centroid size (Zelditch et al., 2004). Positional information is removed by aligning all of the specimens to one another based on their respective landmarks whereas

rotational information is removed by rotating all of the specimens and superimposing them to their mean shape (Zelditch et al., 2004). Therefore, as the mean shape is calculated mathematically it may not represent a specific specimen in the sample (Zelditch et al., 2004, 2012) (see Appendix for further information). This process allows for a comparison between multiple taxa of potentially different size to explore differences in shape by eliminating all non-shape related data, including the bias of size.

After transformation and superimposition, the shape data are analyzed using a statistical method of ordination (i.e., a process of summarizing variation in 2D or 3D space), typically either Principal Components Analysis (PCA) or between-group PCA (bgPCA) and/or sometimes Canonical Variates Analysis (CVA) (Zelditch et al., 2004, 2012; Cooke and Terhune, 2015). While both ordination methods produce new variables that are linear combinations of the original variables, PCA is used for maximizing differences between specimens whereas bgPCA and CVA are used for maximizing differences between groups (Zelditch et al., 2012). However, because CVA defines the shape space based on the number of groups and assumes a homogeneous covariance structure with an invertible matrix to do so, it is used less frequently than PCA or bgPCA, which make fewer assumptions about the data in defining the shape space (Cooke and Terhune, 2015). Additionally, PCA is used to reduce the dimensionality of data (Cooke and Terhune, 2015) such that multidimensional data are more easily visualized in 2D or 3D (Zelditch et al., 2004).

Previous studies have used 2DGM to identify dental remains of extant and fossil specimens to genus and species (Calede and Glusman, 2017; Hulme-Beaman et al., 2018a; Wyatt et al., 2021). These studies have been used to explore taxonomic affinities, phylogenetic signals, and evolutionary histories of various rodent species from around the world (Calede and

Glusman, 2017; Hulme-Beaman et al., 2018a; Wyatt et al., 2021). To test the methodology, both landmarks and semilandmarks have been used in the past which yielded different results depending on the questions asked (Calede and Glusman, 2017; Hulme-Beaman et al., 2018a; Wyatt et al., 2021). Results show that depending on which teeth are used and how many teeth are used, the 2DGM can be successful in taxonomic identifications of isolated teeth and toothrows (Calede and Glusman, 2017; Hulme-Beaman et al., 2018a; Wyatt et al., 2021). Despite the success of 2DGM in these studies for taxonomic identification, there are potential issues that were not investigated such as the effects of image viewing angle (i.e., the position of the object in relation to the camera) and molar wear stage (Gómez-Robles et al., 2007; Calede and Glusman, 2017; Macdonald et al., 2020). While these issues are avoided by only including specimens of similar wear stages and images taken at exact angles, understanding how these issues impact analyses will allow for more robust understanding of archaeological assemblages and rodent taxa.

Objectives

In this study, I use and evaluate the efficacy of 2DGM to quantitatively characterize the sizes and shapes of murine rodent (i.e., rat) mandibular molar rows from the archaeological site of Liang Bua, a limestone cave located on the island of Flores in Indonesia (Figure 1) and the type site of *Homo floresiensis* (Brown et al., 2004). Liang Bua preserves a rich faunal assemblage that spans the past ~190 thousand years (Sutikna et al., 2016, 2018). This assemblage, which to date includes more than 280,000 identified skeletal/dental elements of mammals, birds, reptiles, and mollusks, provides a potential wealth of information about the paleoecology of western Flores (van den Bergh et al., 2009; Sutikna et al., 2018; Veatch et al.,

2019). Rats make up ~78% of 284,689 identified elements at the site (Sutikna et al., 2018) and include at least seven genera and at least eight species that are endemic[3] to Flores (van den Bergh et al., 2009; Locatelli et al., 2012, 2015; Veatch et al., 2019; Veatch, 2021). Among these endemic taxa, body mass varies greatly and includes giant (~1200–2500 g), huge (~600–1600 g), large (~300–600 g), medium (~100–300 g), and small-bodied (≤ 100 g) rats (Veatch et al., 2019). *Papagomys armandvillei,* the largest murine species known on Flores, is still extant (Musser, 1981) and is the only taxon that falls within the giant size category (Veatch et al., 2019). Huge taxa include *Papagomys theodorverhoeveni* and *Spelaeomys florensis*, both of which are presumed extinct (Musser et al., 1981; van den Bergh et al., 2009; Veatch et al., 2019). *Hooijeromys* cf. *nusatenggara* is another species presumed extinct and it had a large body size (Veatch et al., 2019). Liang Bua also preserves evidence of two medium-bodied species, *Komodomys rintjanus* and *Paulamys naso*, and two small-bodied species, *Rattus hainaldi* and *Rattus exulans* (Musser, 1981; Musser et al., 1986; van den Bergh et al., 2009; Locatelli, 2010; Thomson et al., 2014; Locatelli et al., 2015; Veatch et al., 2019).

Due to the sheer quantity of murine remains recovered at this site (Sutikna et al., 2018; Veatch et al., 2019), it is imperative to have robust methods for determining the taxonomic composition of the assemblage at Liang Bua. As many of these species are presumed extinct or extirpated, teeth and jaws are integral to any taxonomic assessments of these archaeologically recovered materials. This is particularly the case for *Papagomys theodorverhoeveni*, *Spelaeomys florensis*, and *Hooijeromys* cf. *nusatenggara*, all of which are known solely from dentognathic remains (Musser, 1981; Veatch et al., 2019). As a quantitative and visualization method, 2DGM offers a potentially useful resource for assessing taxonomy within the Liang Bua murine assemblage. Although the dentition of species included in this study have all been documented

and described previously (Hooijer, 1957, Musser and Boeadi, 1980; Musser, 1981; Musser et al., 1986; Kitchener et al., 1991a,b) variation within the Liang Bua assemblage that is not captured in these descriptions makes it difficult for non-experts to reliably identify species based on these descriptions alone. Furthermore, the 2DGM provides a favourable method for assessing taxonomy because it can avoid some of the pitfalls associated with an archaeological sample of this nature. Occlusal patterns, for example, can sometimes be obfuscated by sediment and rendered ineffectual for taxonomic identification. Additionally, parts of the occlusal surface may be obliterated by wear or broken, making the occlusal surface insufficient for confidently assessing taxonomy. Accurate taxonomic assessments are integral to reconstructions of the paleoecology of Liang Bua and Flores as previous research suggests that the murine taxa exhibit morphological adaptations for different habitats. Quantitative methods are a great addition to this challenging process. Therefore, in this study I investigate the following research questions:

1) Can 2DGM reliably distinguish the endemic Flores murines from one another using images of the mandibular molar rows from the holotypes[4] and/or other well documented specimens (e.g., wild caught animals in which no doubt surrounds their species identification), and if so,

2) Can 2DGM reasonably identify these taxa in the Liang Bua archaeological assemblage using images of the mandibular molar rows?

3) In addition, what are the effects of the image viewing angle and molar wear stage on the 2DGM analysis and, if significant, how can these be mitigated?

Methods

Samples

The study sample consists of 196 images of complete mandibular molar rows (i.e., all three molars present) obtained from published and unpublished sources (Table 1). Only images that included a reasonably clear and direct view of the occlusal surface of at least the first two mandibular molars were selected for analysis. This criterion was important because all three molars may not always be in the same occlusal plane as one another due to taphonomic processes and/or natural differences in the orientation within the alveoli of individual molars, and this is often the case for the third molar. All images were analyzed as if the toothrow was from the right side; left toothrow images were mirrored using Adobe Photoshop version 19 (Adobe, 2018).

Mandibular molar row images of the following holotype specimens were obtained from published sources: RMNH 18301 (*Papagomys armandvillei*), "Specimen 12" (*Papagomys theodorverhoeveni*), "Specimen 1" (*Paulamys naso*), and WAM-M32877 (*Rattus hainaldi*) (Musser, 1981; Kitchener et al., 1991a). Published images for the holotypes of *Rattus exulans* and *Komodomys rintjanus* were either not available or not suitable for analysis and were therefore substituted with those of well documented and museum accessioned wild caught specimens (WAM-M32609 and MZB-9014, respectively) (Musser, 1981; Kitchener et al., 1991a). The holotypes of *Spelaeomys florensis* and *Hooijeromys nusatenggara* are both maxillary tooth rows, thus mandibular remains from similarly aged deposits from the same localities (Liang Toge ("Specimen 1") and the So'a Basin (F2494), respectively) as the holotypes were used instead (Hooijer, 1957).

An additional 21 mandibular molar row images of modern and archaeological specimens for which species identification was confidently assessed using a variety of methods (e.g.,

external and internal anatomy) were obtained from a combination of published (Hooijer, 1957; Musser, 1981; Musser et al., 1986; Kitchener 1991b) and unpublished sources (provided by Drs. E. Grace Veatch, Kristofer Helgen, and Matt Tocheri). Finally, 144 unpublished mandibular molar row images (provided by Drs. E. Grace Veatch and Matt Tocheri) and 19 images from published sources (Locatelli, 2010; Locatelli et al., 2012, 2015) of archaeological specimens from Liang Bua were obtained, and supplemented with four published scientific illustrations of archaeological specimens from Liang Toge and a modern specimen of *Paulamys naso* (Musser, 1981; Kitchener et al., 1991a). When possible, the unpublished images were taken using a Dino-Lite (Model AM7915MZT) digital microscope securely positioned on a stand. To broaden the sample, however, images taken using other digital devices were also included provided the image quality and viewing angle were adequate and met the criterion described above.

2D Geometric Morphometric Analysis

To compare the holotype or reasonable substitute of each species with one another as well as the 21 modern and archaeological specimens with known taxonomy, a set of 17 landmarks representing reasonably homologous structures for these taxa was selected to capture variation in the overall dimensions and shape of each molar in the toothrow as well as the relative positions of individual cusps, as described by Musser (1981) (Figure 2). The first, second, and third molars have seven, five, and five landmarks, respectively, and the anatomical locations of each landmark are described in Table 2. Landmarks were deliberately positioned around the outline of each molar to minimize the effects of occlusal wear and/or taphonomic damage (e.g., erosion due to avian digestion) as much as possible. All molars were required to be fully intact at the landmark locations (i.e., no chips or breaks where a landmark would normally be situated). As

19

the endemic Flores rats exhibit considerable variation in body and tooth size (Musser, 1981; Veatch et al., 2019), the centroid size of each specimen of known taxonomy was calculated based on the landmark set as a measure of overall size. Although some of the images for the Liang Bua archaeological sample did not include suitable scales and thus, centroid size could not be included as a size variable, it was still straightforward to divide the sample into three size categories (i.e., small, medium, and larger-sized rats) based on previous work (Musser, 1981; Veatch et al., 2019) for further shape analyses. Moreover, although centroid size is a useful metric, it is not required to assess shape differences between taxa. For the shape analyses of the medium-sized rats (~100–300 g) and small-sized rats (≤ 100), which included *Paulamys naso*, *Komodomys rintjanus*, *Rattus hainaldi*, and *Rattus exulans*, an additional landmark (#6) was added to the first molar (Figure 2A). For the shape analyses of the larger-sized rats (~600–2500 g), which included *Spelaeomys florensis*, *Papagomys armandvillei*, *Papagomys theodorverhoeveni*, and *Hooijeromys* cf. *nusatenggara*, 18 landmarks were also used but because *Papagomys armandvillei* does not typically have a posterior labial cusplet on its first molar (Musser, 1981), landmark six was shifted posteriorly to the third lamina and positioned on the most labial aspect of the hypoconid (Figure 2B).

Landmarks were digitized using tpsUTIL32 (Rohlf, 2021) and tpsDIG2w32 (Rohlf, 2018), which are part of the Stony Brook morphometrics software suite, with all subsequent analyses performed in RStudio version 3.6.1 (RStudio Team, 2019). All landmarks were exported from tpsDIG2w32 as a .tps file in x, y format and imported into RStudio for data analysis and visualization using the Geomorph package, version 3.1.3 (Adams et al., 2019). To remove size, position, and rotational information in each analysis, the landmark coordinates of all specimens were aligned and scaled to the same size as well as superimposed to a common

reference shape using generalized Procrustes analysis (Zelditch et al., 2004, 2012; Slice, 2005). Creation of the common reference shape is an iterative process that minimizes the average distances between each shape (in this case, the shape of the mandibular toothrow) and the reference shape (Zelditch et al., 2012). After the x, y coordinate data were transformed into shape data by the generalized Procrustes analysis, PCA was used to ordinate and reduce the dimensionality of the shape data as well as visualize the distribution of specimens within the shape space (Zelditch et al., 2004). Although there are other methods of ordination, PCA was used to highlight the differences between individuals since it is relatively assumption free and requires no *a priori* defined group information.

Effects of image viewing angle and molar wear stage on the 2DGM analyses

Only images that included a reasonably clear and direct view of the occlusal surface of at least the first two mandibular molars were included in this study. However, the viewing angle of the toothrow's occlusal plane varied considerably among the selected study sample. This variation was typically the result of either the camera angle relative to the toothrow and/or the set of the individual molars within the dentary, which can be affected by numerous factors (e.g., genetics, taphonomy, etc.). Therefore, to investigate the effects of image viewing angle on the 2DGM analyses, additional images of 25 medium-sized specimens were taken at five angles (anterior, posterior, buccal, lingual, and occlusal) and compared separately. All of these images were taken using a Dino-Lite (Model AM7915MZT) digital microscope positioned on a stand at a 90° angle from the specimen. It should be emphasized that all of these viewing angles reasonably captured the occlusal surface of the toothrow and thus met the criterion for inclusion in this study. This was done intentionally to replicate and slightly extend the expected variation

in image viewing angle present in the comparative study sample. A set of 18 landmarks (Figure 2A) was used and placed in the defined locations (Table 2) irrespective of the image viewing angle (e.g., the landmark for the most lingual aspect of the anterior-lingual cusp was placed on the most lingual aspect visible in the image). This variation in the placement of the landmarks among the images of each specimen should reasonably replicate the variation present among the larger study sample.

Rats in the medium size category formed the largest component of the study sample overall and the giant rat, *Papagomys armandvillei*, had the largest number of confirmed (either published or museum accessioned) specimens identified to species level prior to the analysis. Thus, specimens of medium-sized taxa and *Papagomys armandvillei* were used to investigate the effects of tooth wear on the 2DGM analyses. Each specimen was scored using five wear stages, descriptions of which are defined in Table 3 and were based on the consistently observed wear pattern of the main cusps (Figures 3 and 4). After scoring for wear stage, a set of 18 landmarks was used for both the medium-sized rats (*Komodomys rintjanus* and *Paulamys naso*) (Figure 2A) and *Papagomys armandvillei* (Figure 2B) samples. Finally, the landmark data for the image viewing angle and molar wear stage samples were subject to 2DGM analyses with PCAs used to visualize the ordinated shape data while a Procrustes analysis of variance (ANOVA) was used to test for statistically significant differences among viewing angles and wear stages, respectively.

Results

Holotypes or Reasonable Substitutes

Not surprisingly, centroid size distinguished the smallest species (*Rattus hainaldi* and *Rattus exulans*) on one end and the largest species (*Papagomys armandvillei*, *Papagomys*

theodorverhoeveni, and *Spelaeomys florensis*) on the other among the holotypes or reasonable

substitutes (Figure 5A). The medium-bodied species (*Komodomys rintjanus* and *Paulamys naso*)

were also clearly separated from the larger-bodied *Hooijeromys nusatenggara* based on centroid

size.

For the 2DGM shape comparisons, PC1 explained 45% of the variance and distinctly

separated *Spelaeomys florensis* from the other Liang Bua taxa (Figure 5B). The thin plate splines

displayed a notably more narrow and mesiodistally elongated toothrow in *Spelaeomys florensis*

in comparison to the other taxa. This result was driven by the fact that *Spelaeomys florensis* has

relatively narrow molars when the auxiliary cusplets are excluded from consideration (Figure 6).

Additionally, the individual molars were narrow and long with none being particularly wider

than the others whereas, relative to *Spelaeomys florensis,* all other taxa had shorter molar rows

with shorter individual molars with differing widths. There were also striking differences in how

the first and second molars articulated with one another. In *Spelaeomys florensis*, there was a

substantial gap between the first and second molars resulting in the latter having the appearance

of being angled distally in the thin plate spline. This differed from *Papagomys armandvillei*, for

example, which exhibited a second molar that extended mesially to articulate with the first molar.

In other words, the anterior labial cusplet of the second molar extended mesially and was

positioned buccally relative to the posterior cingulum of the first molar. Along with this mesial

extension of the anterior labial cusplet, the protoconid also extended mesially relative to the rest

of the second molar. This condition differed from that in *Spelaeomys florensis* where the

protoconid was transverse to the metaconid with no mesial extension. Lastly, the third molar of

Spelaeomys florensis was also notably narrower and more elongated than that of the other taxa

despite the fact that this tooth typically showed more variation in how it was positioned in the mandible.

As almost half of the total variance was due to shape differences between *Spelaeomys florensis* and all the other taxa, the subsequent PCs mainly documented shape variation among the other taxa. On PC2, which explained 21% of the variance, the largest species (*Papagomys armandvillei*) was again separated from the two smallest ones (*Rattus hainaldi* and *Rattus exulans*) but based on the distribution of the other taxa along this axis it is clear that PC2 is driven by shape rather than size variation. Indeed, the thin plate splines for PC2 showed that it captures variation in molar lengths relative to widths (Figure 5C). In this respect, the two small *Rattus* species had exceptionally elongated molars relative to molar width in comparison to *Papagomys armandvillei*, which displayed a relatively shorter molar row. Other differences between these taxa in their overall toothrow shape included small *Rattus* exhibiting a slightly narrower toothrow, especially the first and second molars, than *Papagomys armandvillei*. Furthermore, the most labial aspect of the first molar in small *Rattus* was positioned more mesially relative to the corresponding lingual landmarks. In *Papagomys armandvillei*, the first lamina of the first molar was largely symmetrical with similarly sized and positioned anterior labial and anterior lingual cusps. This condition differed from the first lamina of the first molar in the small *Rattus* wherein the anterior labial cusp was positioned more distally relative to the anterior lingual cusp. Additionally, as shown in the thin plate splines for PC2, the relative size of the anterior lingual cusp of *Papagomys armandvillei* was notably larger than that of small *Rattus*. Strikingly, the larger-bodied rats were still separated from one another relatively well along PC2 with *Papagomys armandvillei* plotting most negatively, *Hooijeromys nusatenggara* plotting most positively, and with *Papagomys theodorverhoeveni* and *Spelaeomys florensis* in between these

two extremes. However, there was no clear separation between either the small-bodied rats or the medium-bodied rats along PC2.

On PC3, which explained 13% of the total variance, *Paulamys naso* plotted furthest negatively whereas *Hooijeromys nusatenggara* plotted furthest positively ([Figure 5D](#)). However, the small-bodied taxa, *Rattus hainaldi* and *Rattus exulans*, were also well separated from one another along this axis as were the medium-bodied taxa, *Komodomys rintjanus* and *Paulamys naso* ([Figure 5D](#)). The thin plate splines revealed that the variation along PC3 was due mostly to differences in the relative widths in the first and second molars. In taxa that plotted positively along this axis (*Hooijeromys nusatenggara*, *Komodomys rintjanus*, and *Rattus exulans*), the second molar was relatively wider than the first molar in comparison to taxa that plotted more negatively (*Paulamys naso* and *Rattus hainaldi*). Furthermore, PC3 also separated *Papagomys armandvillei* from *Papagomys theodorverhoeveni*; however, this separation was less pronounced than the observed differences between the small- and medium-bodied species.

Confirmed Museum Specimens

Additional known specimens provided further clarity into how these taxa compare with one another in terms of their mandibular toothrows. Centroid size again distinguished clearly between the different size classes with the small-bodied rats on one end and *Papagomys armandvillei* on the other ([Figure 7A](#)). On PC1, which explained 38% of the total variance, *Spelaeomys florensis* again clearly deviated from the rest of the Liang Bua taxa based on its narrower (when the auxiliary cusplets are excluded) and more mesiodistally elongated molars ([Figure 7B](#)). In contrast, the other Flores taxa had molars that were wider and more mesiodistally compressed relative to those of *Spelaeomys florensis*. This was especially true for *Komodomys*

rintjanus, which plotted furthest negatively on PC1. Additionally, in *Komodomys rintjanus* the first two molars fit together by the anterior labial cusplet of the second molar, which is positioned laterally to the posterior cingulum of the first molar. In other words, there was little to no gap between the first two molars as they were positioned so closely to one another. This differed from the condition in *Spelaeomys florensis*, which displayed a notable gap between the first two molars (Figure 7B). In the thin plate splines, the posterior cingulum of *Spelaeomys florensis* was positioned posteriorly relative to the reference specimen.

PC2, which explained 15% of the total variance, was again driven by a shape comparison between *Rattus hainaldi* (negative) and *Papagomys armandvillei* (positive) (Figure 7C). Relative to *Papagomys armandvillei*, *Rattus hainaldi* had an elongated and narrow toothrow with the second molar notably wider than the first. Additionally, the overall shape of the first molar in *Papagomys armandvillei* differed due to the increased relative size of the anterior lingual cusp. In *Rattus hainaldi*, this cusp was approximately the same size as the anterior labial cusp and accounted for the different shape of the first lamina in the two thin plate splines (e.g., a greater distance between the two landmarks on the anterior lingual cusp indicate a relatively larger cusp). Moreover, the anterior labial cusp on the second molar of *Papagomys armandvillei* protruded mesially and was positioned lateral to the posterior cingulum of the first molar with little to no space between the two. The mesial positioning of this cusp was also seen in *Rattus hainaldi*; however, there was a larger space between it and the posterior cingulum.

On PC3, which explained 9% of the total variance, both *Papagomys armandvillei* and *Komodomys rintjanus* spanned nearly the entire axis due to slight differences primarily in the second molar and orientation of the first lamina in the first molar; however, this variation did not contribute to differentiating among the taxa (Figure 7D). This high level of intra-species

variation in *Papagomys armandvillei* and *Komodomys rintjanus* was notable but may be influenced by the effects of wear stage and/or image viewing angle, both of which are examined in detail further below.

In total, the 2DGM analyses thus far showed promising results in terms of distinguishing between each of the endemic Flores taxa based on a combination of mandibular molar shape and size. Given that centroid size clearly separated these taxa into previously recognized body size classes, subsequent shape analyses in this study were performed separately on the small, medium, and larger-bodied categories to focus more specifically on the shape variation present within each size class.

Small-bodied Archaeological Specimens From Liang Bua

The two small-bodied taxa thought to be represented in the Liang Bua assemblage are *Rattus hainaldi* and *Rattus exulans*. Within the holotypes and confirmed specimens analysis, there is moderate separation between the two; however, with the addition of the rest of the small-bodied specimens, there was no definitive separation between the two taxa. On PC1 (Figure 8), which explained 21% of the total variance, the holotype for *Rattus hainaldi* and the reasonable substitute for *Rattus exulans* showed some separation with potential clustering surrounding them. PC1 largely captured differences in the first molar with labial landmarks being positioned more distally relative to their lingual counterparts along positive PC1 and more transverse on negative PC1. Though there is separation of the holotypes, other specimens that have been tentatively identified to the species level do not cluster as expected with the holotypes. Along PC2, which explained 18% of the total variance, variation was driven by differences in the relative widths of the molars (Figure 8B). Published descriptions of the two small-bodied taxa

(Kitchener et al., 1991b) suggest that the widths of the molars is significant; however, this difference does not contribute towards separation of known specimens in the shape space.

Medium-bodied Archaeological Specimens From Liang Bua

The two endemic medium-bodied murines found at Liang Bua are *Paulamys naso* and *Komodomys rintjanus*. As was seen in the holotype and other known specimen comparisons, the 2DGM results for the archaeological specimens in this size class captured salient morphological features that distinguished these two taxa from one another. Along PC1, which explained 25% of the total variance, two clusters primarily driven by differences in overall toothrow shape were observed (Figure 9A). Specimens displaying relatively narrow and elongated toothrows plotted negatively along this axis whereas specimens with relatively wider and more mesiodistally compressed toothrows plotted positively. Given the published descriptions of these two species and the plotted positions of the holotypes and other known specimens, the negative and positive clusters almost certainly represent *Paulamys naso* and *Komodomys rintjanus*, respectively. Moreover, in the putative *Komdomys rintjanus* cluster, all of the labial landmarks were located more distally relative to their lingual counterparts. For example, the landmark located on the anterior labial cusp was positioned more distally relative to its counterpart on the anterior lingual cusp. In contrast, landmarks representing individual lamina were oriented more transversely in the negative cluster (i.e., *Paulamys naso*). Another distinction captured by the variation along PC1 was the relative distance between each lamina, particularly on the lingual side, with *Paulamys naso* typically displaying lamina that were more spaced apart relative to those in *Komodomys rintjanus*. Finally, differences in the relative widths of the first and second molar were also captured by PC1. In *Paulamys naso*, the first and second molars were similar in width

to one another. *Komodomys rintjanus*, on the other hand, had a second molar that was markedly wider than the first (Musser, 1981).

All subsequent PCs primarily appeared to capture intra-species variation rather than inter-species variation. Along PC2, which explained 12% of the total variance, both taxa occupied the shape space with *Komodomys rintjanus* driving the variation (Figure 9B). Interestingly, there was less overall variation in the putative *Paulamys naso* cluster along PC2 suggesting that this taxon is less variable than *Komodomys rintjanus* or perhaps that image viewing angle and the degree of wear affected the 2DGM of *Paulamys naso* less than that of *Komodomys rintjanus*. Overall, although there was some overlap between the two clusters along PC1, the 2DGM analysis appeared to effectively distinguish between *Paulamys naso* and *Komodomys rintjanus* providing a useful quantitative method to use in conjunction with qualitative and other quantitative assessments for taxonomic classification of additional medium-bodied specimens from Liang Bua and elsewhere on Flores.

Larger-bodied Archaeological Specimens From Liang Bua

The 2DGM analysis of the larger-bodied taxa, which included *Papagomys armandvillei*, *Papagomys theodorverhoeveni*, *Hooijeromys* cf. *nusatenggara,* and *Spelaeomys florensis*, showed notable differences among these taxa. Although centroid size easily distinguished *Hooijeromys* cf. *nusatenggara* from these other species in the previous analyses (e.g., Figure 7A), this taxon was included in this shape analysis to identify how its shape compares to the other larger-bodied taxa. Along PC1, which explained 33% of the variance, there was a clear distinction between *Spelaeomys florensis* and the other taxa. *Spelaeomys florensis* drove the variation positively along this axis whereas the two *Papagomys* species drove the variation

negatively and *Hooijeromys* cf. *nusatenggara* did not contribute to the variation along PC1 ([Figure 10A](#)). As discussed above, one of the distinguishing features between *Spelaeomys florensis* and the other larger-bodied taxa was how the first and second molars articulated with one another. In *Spelaeomys florensis*, the molars did not articulate tightly with one another as evidenced by the more posterior positioning of the anterior labial cusplet relative to the posterior cingulum. Additionally, the cusps were much more narrow than they were in *Papagomys armandvillei*. While *Spelaeomys florensis* looks wider upon visual inspection, without the numerous auxiliary cusplets, they actually have a significantly more narrow toothrow as was seen in the thin plate spline for positive PC1. Furthermore, the first and second molars were both similar in width in *Spelaeomys florensis* whereas the second molar was relatively wider than the first in the other larger-bodied taxa.

Along PC2, which explained 14% of the variance, there was some separation between *Papagomys armandvillei* and *Papagomys theodorverhoeveni* ([Figure 10B](#)). *Papagomys theodorverhoeveni* drove the variation negatively along this axis whereas *Papagomys armandvillei* drove the variation positively. In *Papagomys theodorverhoeveni*, the mesial part of the second molar protruded labially; thus, the anterior labial cusp of the second molar was positioned more labially relative to the posterior cingulum of the first molar. This resulted in a considerable gap between the landmarks representing these two morphological features and deviated from the condition seen in *Papagomys armandvillei* where the anterior labial cusp of the second molar was positioned closer (more mesially) to the posterior cingulum of the first molar. However, the second molar of *Papagomys armandvillei* was still wider than the first and third molars despite a more mesially positioned anterior labial cusp. Additionally, the most mesial aspect of the first molar's anterior lingual cusp was positioned more lingually in

Papagomys theodorverhoeveni than it was in *Papagomys armandvillei* and the first molar in the former was slightly more elongated than it was in the latter. Thus, the labial landmarks in *Papagomys theodorverhoeveni* were positioned further apart from one another suggesting that the individual lamina of *Papagomys theodorverhoeveni* are individually more mesiodistally elongated than they are in *Papagomys armandvillei*.

PC3, which explained 11% of the variance, captured the intra-species variation in *Papagomys armandvillei* that was observed previously (Figures 10C and 10B) while PC4, which explained 7% of the variance, resulted in some separation between *Hooijeromys* cf. *nusatenggara* and the other larger-bodied taxa (Figure 10D). *Hooijeromys* cf. *nusatenggara* drove the variation positively along this axis whereas *Papagomys armandvillei* drove the variation negatively. The thin plate splines for this axis showed that *Hooijeromys* cf. *nusatenggara* had a first molar that was both long and wide relative to that of *Papagomys armandvillei* but with a strikingly narrow first lamina. In other words, all three laminae in the first molar of *Papagomys armandvillei* were similar in width whereas the anterior lamina in *Hooijeromys* cf. *nusatenggara* was considerably narrower than the other two. Additionally, the second lamina of the first molar and both laminae in the second molar were all rooted more distally in *Hooijeromys* cf. *nusatenggara* (even though the cusp tips were angled more mesially) resulting in larger gaps between the first molar's first and second laminae and between the distal and mesial aspects of the first and second molar, respectively. In contrast, *Papagomys armandvillei* had laminae that flared mesiolabially and had smaller gaps between them.

Overall, the 2DGM analysis of the larger-bodied taxa captured distinctive molar shape differences among these four taxa. *Spelaeomys florensis* was the easiest to distinguish from the other three based on shape. Although *Papagomys armandvillei* and *Papagomys*

theodorverhoeveni were morphologically similar and overlapped with one another in molar size, this analysis was still able to reasonably distinguish between these two taxa. Based on shape alone, *Hooijeromys* cf. *nusatenggara* was the most difficult to distinguish but as noted above, the inclusion of centroid size would rectify this issue.

Effects of image viewing angle on the 2DGM analyses

Using 25 specimens identified either as *Paulamys naso* (n = 13) or *Komodomys rintjanus* (n = 12), each of these specimens was photographed from five viewing angles: buccal, lingual, anterior, posterior, and occlusal (Figure 11). Based on the 2DGM results presented earlier, Figure 12A–C shows the shape differences that result when image angle varies. In *Paulamys naso*, the most extreme differences were observed between buccal and lingual angles, which plot the furthest negatively and positively along PC1 and explained 33% of the total variance, respectively (Figure 12A). The other three angles fall in between these two extremes and separate more along PC2. The thin plate splines representing buccal angles (plotting more negatively along PC1) show a relatively narrower toothrow whereas the lingual viewing angles resulted in a slightly wider toothrow. Furthermore, buccal viewing angles result in the second molar appearing wider than the first whereas it is relatively the same width as the first molar in lingual viewing angles. On PC2, which explains 15% of the total variance, some more subtle differences between the posterior and anterior viewing angles were captured. Posterior viewing angles resulted in more elongated third molars whereas anterior viewing angles resulted in relatively shorter third molars. Using a sequential Bonferroni adjustment for multiple pairwise comparisons, a Procrustes ANOVA indicates that the difference between the buccal and lingual viewing angles is statistically significant (p = 0.001) as is the difference between the anterior and

posterior viewing angles (p = 0.008). Moreover, lingual viewing angles were significantly different from all three other viewing angles (p = 0.001). However, the differences between occlusal and posterior, occlusal and anterior, and occlusal and buccal viewing angles are not statistically significant (p > 0.05).

In *Komodomys rintjanus*, a similar pattern emerged where buccal and lingual viewing angles resulted in relatively narrower and wider molars, respectively. On PC1, which explains 33% of the total variance, buccal viewing angles plot most negatively and lingual angles most positively with occlusal, anterior, and posterior angles plotting in between (Figure 12B). This relative narrowing and widening occurred throughout the toothrow and did not particularly affect one tooth more than the others. Moreover, the differences in the buccal and lingual angles are captured in the relative widths of the first two molars. In the buccal viewing angles, the second molar appears notably wider than both the first and third molars. In the lingual viewing angles, the second molar appears slightly wider than the first molar. As above, the differences between posterior, occlusal, and anterior angles were captured on PC2, which explains 19% of the total variance. The thin plate splines captured differences in the elongation of the individual molars. In the posterior viewing angles, the third molars, and to some extent, the second molars, are relatively elongated; however, this elongation is not seen in the first molars. In the anterior viewing angles, the third molar is severely shortened with some shortening in the second molar. Additionally, there is some elongation of the first molar in the anterior viewing angles. Procrustes ANOVA pairwise comparisons (with sequential Bonferroni adjustment) result in statistically significant differences between the anterior and posterior viewing angles (p = 0.001) and between the buccal and lingual viewing angles (p = 0.001). As above, lingual angles are statistically different from posterior, anterior, and occlusal angles (p = 0.001) and buccal angles

are statistically different from both posterior (p = 0.002) and anterior (p = 0.006) angles. However, buccal angles are not statistically different from occlusal angles (p > 0.05), nor are occlusal angles statistically different from either anterior or posterior angles (p > 0.005).

Effects of molar wear stage on the 2DGM analyses

In the medium-bodied taxa, there were no clustering between the different wear stages within the shape space in the full archaeological sample. Each of the specimens was assigned a wear stage based on the criteria outlined in Table 3 and then each taxa was assessed separately. In *Paulamys naso* (Figure 13A), there is appreciable overlap between the five different wear stages with wear stage one which drove the shape space negatively along PC1, which explained 18% of the variance, and stage three drove the variation positively. Strikingly, stage two specimens occupied a large portion of the shape space and overlapped with all other wear stages. In examining the thin plate splines, negative PC1 represented slightly narrower toothrows than those on positive PC1. Additionally, positive PC1 showed labial landmarks that are slightly more distal relative to the opposing lingual landmarks. Results of Procrustes ANOVA pairwise comparisons (using a sequential Bonferroni adjustment) show that wear stages one (p ≤ 0.003) and two (p = 0.02) are significantly different from other stages.

In *Komodomys rintjanus*, there is substantial overlap between all wear stages (Figure 13B), particularly stages two through four. Wear stage two plots furthest negatively on PC1, which explained 19% of the variance, with stage four plotting most positively; however, both stages span nearly the full length of PC1. On negative PC1, the labial landmarks are positioned more distally relative to the opposing lingual landmarks. This is more notable on the first and second molars, which are also most affected by wear in this sample. Additionally, negative PC1

34

shows a toothrow that is slightly more narrow than positive PC1. Because stages two and four span nearly the whole range of PC1, there is little additional information to be gained from the thin plate splines. In contrast to the wear analysis in *Paulamys naso*, stage one plots largely within the range of variation captured by stages two through four. Stage five, on the other hand, plots primarily on the positive end of PC1 but overlaps with the range of stages two through four. Results of Procrustes ANOVA pairwise comparisons (using a sequential Bonferroni adjustment) show that there are statistically significant differences between stages two and three ($p = 0.001$), two and four ($p = 0.004$), one and three ($p = 0.002$), and one and four ($p = 0.003$). No other statistically significant differences between stages were observed.

In *Papagomys armandvillei*, there were no specimens in the archaeological sample representing the earliest (stage one) and latest (stage five) wear stages and there was substantial overlap between stages two through four (Figure 14). Stage two drives the variation along both positive and negative PC1, which explains 24% of the variance suggesting that this variation is not wear-related but rather intra-species variation, and stages three and four almost completely overlap with one another. Using a sequential Bonferroni adjustment, there are no statistically significant differences between any of these stages ($p > 0.05$)

Discussion

Holotypes or Reasonable Substitutes and Confirmed Museum Specimens

The first goal of this study was to investigate whether 2DGM can reliably distinguish eight of the endemic murine species on Flores from one another using images of their mandibular molar rows. Using holotype and/or other well documented specimens (e.g., modern or archaeological specimens in which no doubt surrounds their species identification), the results

suggested that mandibular toothrows of each of these taxa are reasonably identifiable using a combination of size and shape, consistent with previous qualitative and quantitative studies of these species (Hooijer, 1957; Musser, 1981; Musser et al., 1986; Locatelli, 2010; Locatelli et al., 2012, 2015; Veatch, 2014; Veatch et al., 2019). Centroid size by itself clearly separated the smallest species (*Rattus exulans* and *Rattus hainaldi*) from the medium-bodied ones (*Komodomys rintjanus* and *Paulamys naso*), which in turn are clearly separated from *Hooijeromys nusatenggara* and the three larger-bodied taxa (Figures 5A and 7A). The holotype of *Papagomys armandvillei* has a centroid size comparable to that of the *Spelaeomys florensis* specimens and was larger than that of the *Papagomys theodorverhoeveni* holotype. However, some of the other *Papagomys armandvillei* specimens had centroid sizes that are similar to those of *Papagomys theodorverhoeveni*. Thus, although centroid size distinguishes the three largest species from all the others, it did not appear sufficient to reliably distinguish among them.

Among the small rats, *Rattus hainaldi* displayed a second molar that is narrower relative to its first molar in comparison to that of *Rattus exulans*. However, as only two documented specimens were available for this size class, it remains unclear whether this shape feature truly represents a species-level difference. However, *Paulamys naso* also typically displays a second molar that is not as wide relative to its first molar in comparison to that of *Komodomys rintjanus* and this difference in molar proportions is maintained in the 2DGM analyses with additional medium-bodied specimens, especially the Liang Bua archaeological sample.

Among the three largest taxa, *Spelaeomys florensis* has highly distinctive molar shapes that drive the variation along PC1 of every analysis in which this species was included. Its molars are "highly cuspidate" and include many high cusped and large auxiliary cusplets, particularly on the labial side of each tooth (Musser, 1981:110). Compared to the two

Papagomys taxa, without its labial auxiliary cusplets the molars of *Spelaeomys florensis* were considerably narrower. Shape differences between the two *Papagomys* species captured by the 2DGM analyses included a relatively elongated toothrow in *Papagomys theodorverhoeveni* due to the fact that the rows of cusps are set further apart from one another than in *Papagomys armandvillei* (Musser, 1981). Other more qualitative features also distinguished these two taxa from one another but the configuration of the selected landmark set used in this study failed to capture these features (particularly subtle differences in the occlusal surfaces). For example, in *Papagomys theodorverhoeveni*, the first lamina is composed of a prominent anterior lingual cusp that is substantially larger than the opposing anterior labial cusp and more angular in its outline (Musser, 1981). In *Papagomys armandvillei*, the anterior lingual cusp is also larger than the anterior labial cusp; however, the shape differs from that of *Papagomys theodorverhoeveni* in such a way that it appears more "tear drop" shaped (Musser, 1981:96). In addition to the anterior lingual and anterior labial cusps, *Papagomys theodorverhoeveni* also presents with an anterior central cusp that is not typically present in *Papagomys armandvillei* and the cusps are set more erect with a more complex occlusal pattern (Musser, 1981). As these additional features are well-documented and quite distinct between these two taxa, future work should aim to develop a specific landmark and/or outline set that aims to delineate only between these two *Papagomys* species.

Archaeological Specimens From Liang Bua

The second goal of this study was to investigate whether 2DGM can reasonably identify these eight endemic Flores murines in the archaeological assemblage from Liang Bua. Overall, the results were extremely promising and this technique provides a valuable resource for Flores

murine taxonomic identification, especially when used in combination with visual inspection and qualitative assessment as well as other quantitative data. For example, the ability to accurately differentiate between the two medium-bodied taxa found at Liang Bua, *Paulamys naso* and *Komodomys rintjanus*, will facilitate further paleoecological reconstructions of the site. These two species are known to prefer different habitats with *Paulamys naso* preferring a more forested or semi-forested environment (Musser, 1981; Musser et al., 1986; Veatch, 2014, 2021; Veatch et al., 2019) whereas *Komodomys rintjanus* prefers a grassland or semi-grassland environment (Sody, 1941; Musser and Boeadi, 1980; Veatch, 2014, 2021; Veatch et al., 2019). Differences in these environments reflect the heterogeneity of the surrounding area and whether it is dominated by grasses or more leafy trees and shrubs.

Being able to reliably and confidently identify between the murine taxa is just the first step in much of the ongoing taphonomic and paleoecological work at Liang Bua. Since these two medium-bodied taxa have known habitat preferences, if either *Paulamys naso* or *Komodomys rintjanus* is found to be predominant in any given layer, inferences can be made about the environment during that time based on the species' known preferred habitat. Previous work on murine long bones suggests that shifts occurred throughout the lifetime of the cave (Veatch, 2021) and the accurate classifications of the dental remains will aid in these reconstructions. Furthermore, most of the accumulation of murine remains at Liang Bua have been attributed to deposits from raptor pellets (Veatch, 2021). Barn owls have a radius of approximately three kilometers around their roosting area (Purger and Szép, 2022) and thus the accumulation of each taxa in a layer should be reflective of the nearby surrounding area. Using these types of reconstructions will also allow for a better understanding of the environment of *Homo floresiensis*.

In the 2DGM analyses, *Paulamys naso* was reasonably distinguished from *Komodomys rintjanus*. Because the occlusal surfaces of these two *Rattus*-like taxa share many morphological similarities (Musser, 1981), particularly in young, unworn specimens, the ability of the 2DGM analyses to differentiate between the two taxa is remarkable. Moreover, the analyses excelled at capturing the distinct relative proportions of the teeth in each taxon. This was especially true for the relative widths of the molars, which appeared consistent throughout the sample regardless of image angle and/or wear stage. Despite the striking separation between the medium-bodied taxa, there was still some overlap between the two. While this may be a result of image angle in some cases, there is some variation within the relative widths of the first and second molars in *Paulamys naso* with the second molar sometimes wider than expected. Although *Komodomys rintjanus* displays more variation as a species, the variation in *Paulamys naso* cannot be discounted. This variation can contribute to difficulties differentiating between the two taxa; however, the combination of qualitative evaluation and the 2DGM provides a strong approach for taxonomic assessment.

In the larger-bodied taxa, the 2DGM analysis also captured distinct differences among the taxa although there was more overlap observed between some of the species. As in the previous analyses, *Spelaeomys florensis* was easily distinguished from the other larger-bodied taxa. However, unlike in the medium-bodied murines, the relative widths of the first and second molars in the two *Papagomys* species were not as distinct from one another and overall there were more similarities in their respective toothrow shapes. Nonetheless, PC2 was essentially a comparison between these two congeners[5] with *Papagomys theodorverhoeveni* and *Papagomys armandvillei* clustered more negatively and positively along this axis, respectively. In the 2DGM analysis, the two *Papagomys* taxa were primarily separated by the positioning of the landmarks

on the first molar. In *Papagomys theodorverhoeveni*, the lamina appeared more mesiodistally

elongated; however, this was likely a result of the known positioning of the cusp rows being set

further apart. In *Papagomys armandvillei*, the lamina are "chevron" shaped (Musser, 1981:82)

and are not set as far apart as in *Papagomys theodorverhoeveni*. This difference in lamina

positioning is captured by the 2DGM and is used to separate the two congeners. Additionally,

linear measurements suggest that there is a molar size difference between these two taxa,

although with some overlap in their respective ranges of variation (Musser, 1981; Locatelli et al.,

2012). In the 2DGM analysis of confirmed specimens, the centroid sizes of the *Papagomys*

theodorverhoeveni specimens overlapped slightly with those of the smaller *Papagomys*

armandvillei specimens, while those of *Hooijeromys* cf. *nusatenggara* easily distinguished it

from the other larger-bodied species and the two medium-bodied taxa as well. If these patterns in

relative size are maintained within larger samples, then the combination of centroid size and the

shape differences captured on PC2 and PC4 (that captured that the lower molars of *Hooijeromys*

cf. *nusatenggara* appeared wider relative to their lengths compared with those of *Papagomys*)

would likely provide clearer separation between these three taxa.

The 2DGM analyses of the smaller-bodied specimens did not yield results that suggested

the Liang Bua sample can be reasonably divided into clusters representing *Rattus exulans* and

Rattus hainaldi. As only two confirmed specimens were available and published descriptions

detailing how the molars of these two taxa differ from one another were limited, future research

should include additional confirmed specimens to ensure that these two taxa can indeed be

differentiated from one another based on mandibular molar shapes.

Overall, the 2DGM methodology and landmark configuration used in this study was

largely successful in differentiating between the various endemic murine taxa from Flores ([Table

6). The separation between taxa, most notably the medium-bodied taxa, is striking, even though the main landmark configuration only captured a subset of the total variation present in the sample. This further demonstrates that pristine specimens are not required and that this methodology is useful for differentiating murine specimens with morphologies that are obscured by sediment. Additionally, though the 2DGM highlighted the morphological differences between the four larger-bodied taxa, the inclusion of size and other qualitative traits in taxonomic classification will help to provide further clarity. Although there were varying degrees of overlap between taxa in certain aspects of the shape space, it is clear that the 2DGM results offer important information about mandibular toothrow size and shape that can be used in conjunction with qualitative and other quantitative data for species identifications of murine specimens from archaeological contexts on Flores.

Effects of image viewing angle and tooth wear on the 2DGM analyses

The third goal of this study was to investigate the effects of image viewing angle and molar wear on the 2DGM analysis and, if significant, how these effects can be mitigated in future work. In particular, it was important to investigate how the selected landmark configuration was affected by the image angle for individual specimens. In examining the results of the Procrustes ANOVA pairwise comparisons it is clear that for both *Paulamys naso* and *Komodomys rintjanus*, images taken from lingual angles are the least appropriate for analysis and should be avoided whenever possible. The reason is because lingual angles tend to completely obfuscate the buccal side of the tooth resulting in distortions to the landmark configuration. Buccal angles were found to be less problematic than the lingual ones, especially for some species (e.g., *Komodomys rintjanus*), because even in images clearly taken from a severe angle,

41

it was still possible to see (and landmark) the lingual side of the tooth. Nonetheless, the results showed that buccal angles are less preferable to occlusal, anterior, or posterior angles. Clear occlusal angles are ideal but anterior and posterior angles do not appear to adversely affect the 2DGM analyses and overlap substantially with images taken from occlusal angles. As anterior and posterior angles result in rather subtle changes to the landmark configurations in comparison to those from direct occlusal views, all three of these angles should be considered reasonably appropriate for future analyses.

When both image angle datasets were analyzed together, an interesting pattern emerged (Figure 12C). On PC1, which described 27% of the total variance, both *Paulamys naso* and *Komodomys rintjanus* formed separate clusters for each image angle but a noticeable gradation (buccal to posterior to occlusal to anterior to lingual) within each species occurs along this axis with each of the five viewing angles plotting successively more negatively. The same pattern is also observed along PC2, which explained 16% of the total variance. A relatively clear distinction between *Paulamys naso* and *Komodomys rintjanus* was still observed through a combination of PC1 and PC2, but on either axis there was overlap that is the result of the different viewing angles. For example, buccal viewing angles cause the second molar in *Paulamys naso* to appear wider than the first, making the toothrow appear more like that of *Komodomys rintjanus* in an occlusal viewing angle. In contrast, lingual viewing angles cause the relative widths of the first two molars in *Komodomys rintjanus* to appear more like that of *Paulamys naso* in an occlusal viewing angle. In comparison to all of the *Paulamys naso* and *Komodomys rintjanus* images used in this study, this image viewing angle analysis shows that the bulk of the study sample is likely composed of occlusal, anterior, and posterior angles. Thus, as noted for the viewing angle analyses for each of these medium taxa, future work should

ensure that lingual and buccal angles are not included in the study sample because they result in distorted landmark configurations that compromise the ability to correctly distinguish these two taxa from one another.

The third goal of this study also sought to understand the effects of tooth wear on the 2DGM results. In both *Paulamys naso* and *Komodomys rintjanus*, the wear stages are reasonably visually distinctive; however, the 2DGM results show that there is substantial overlap between them. Without visual identifications, the 2DGM cannot differentiate between the wear stages due to considerable overlap between the wear stages. Although the difference between stages one and five is statistically significant in both *Paulamys naso* and *Komodomys rintjanus*, this is not easily interpreted from the plots. Visually, all of the wear stages are distinctive and there are subtle, but consistent, differences between all of the stages (Table 4). These stages can be used to visually differentiate between the wear stages in each of the medium-bodied taxa where the 2DGM analyses suggest intra-species variation. These visual identifications can be useful at the early wear stages to differentiate between the medium-bodied taxa as their similar cusp morphologies obscure visual identifications. Similar, more specific, descriptions can be used to identify *Papagomys armandvillei* (Table 5) where the 2DGM shows little difference and no statistical significance. While the 2DGM analysis does consistently separate the taxa, these wear stage descriptions can add to the toolkit that can be used in the field to distinguish between the two species. Additionally, the descriptions of the wear stage are useful for separating the specimens that appear more intermediate on the plot and/or exhibit features that do not distinctly belong to one species or the other.

Although significant differences between some of the wear stages were observed in the medium-bodied taxa, none of the differences were significant in *Papagomys armandvillei*. Most

importantly, wear stage did not appear to have a major effect on the 2DGM analyses that aimed to differentiate between the various Flores taxa. In other words, molar wear stage mainly results in intra-species variation. Although tooth wear must always be considered a limitation for 2DGM studies of teeth (Calede and Glusman, 2017; Hulme-Beaman et al., 2018a, b), the results of this study suggest that for the endemic murines of Flores the inclusion of toothrows exhibiting different stages of wear is reasonable.

Conclusions and Recommendations for Further Research

Overall, this study shows the potential of using 2DGM to help identify endemic Flores murine species based on mandibular toothrow morphology. Although the main landmark configuration used in this study only captured a subset of the total variation present in the sample, the 2DGM analyses were relatively successful in distinguishing the various taxa from one another, particularly in the medium and larger-bodied categories. Future analysis of cusp shape using additional/alternate landmarks, sliding semilandmarks, and/or outlines may provide further insights into the morphological variation of these eight murine species. Further work should also include additional confirmed *Rattus exulans* and *Rattus hainaldi* specimens to investigate whether 2DGM can help differentiate between the mandibular toothrows of these two small-bodied taxa.

Although similar previous studies have had success in identifying specimens to the genus or species level using both landmarks and semilandmarks (Hulme-Beaman et al., 2018a, b), the substantial morphological similarities between the Liang Bua taxa warranted concern about whether the 2DGM would capture the subtle differences between taxa using only landmarks. Results of this study suggest that the 2DGM is able to successfully capture even the most subtle

differences and highlight how the taxa differ from one another. Although this study differs from previous work in the teeth chosen to be landmarked and by only using landmarks, it proved to be a successful approach. This means that although semilandmarks could be used in future work, the landmarks alone provide sufficient information for taxonomic classification in the Liang Bua assemblage. Additionally, since it is common to only use specimens of similar wear stages in 2DGM analyses (Calede and Glusman, 2017; Hulme-Beaman et al., 2018a; Wyatt et al., 2021), this study suggests that including different wear stages can be beneficial, particularly if your sample includes specimens at varying stages of wear. While the 2DGM highlights slight morphological variation, the main identifying features found in the overall morphology remain present and consistent throughout.

Despite the appreciable inter- and intra-species variation observed within the Liang Bua murine assemblage, this study demonstrates that 2DGM provides a powerful tool for identifying and differentiating between taxa, particularly when used in conjunction with qualitative and other quantitative data. Moreover, the results suggest that the effects of image viewing angle and molar wear stage can be mitigated by avoiding lingual and buccal angles as well as using the landmark configuration used in this study. Furthermore, the results of this study suggest that the 2DGM can be useful to make new taxonomic identifications of previously unidentified specimens, confirm and/or refute previous identifications, and provide further support for taxonomic identifications made based on qualitative traits alone. This in turn will further contribute to understanding the paleoecology at Liang Bua in addition to better understanding the small mammal populations that make up such a large part of the site's faunal assemblage.

Tables

Table 1. Breakdown of the study sample. ([back to text]())

Taxa	Images	
	Published	Unpublished
Papagomys armandvillei	4	9
Papagomys theodorverhoeveni	2	0
Spelaeomys florensis	4	0
Hooijeromys cf. *nusatenggara*	0	1
Paulamys naso	3	0
Komodomys rintjanus	4	0
Rattus hainaldi	1	0
Rattus exulans	1	0
Archaeological Specimens		
larger-bodied[1]	7	31
medium-bodied[2]	12	93
small-bodied[3]	5	16

[1] *Papagomys armandvillei, Papagomys theodorverhoeveni, Spelaeomys florensis,* and *Hooijeromys* cf. *nusatenggara*

[2] *Paulamys naso* and *Komodomys rintjanus*

[3] *Rattus hainaldi* and *Rattus exulans*

Table 2. Landmark locations for primary landmark protocol including 18 landmarks. For visual representation, see Figure 2. ([back to text](#))

Molar	Landmarks	
	Number	Description
M1	1	Most anterior aspect of the anterior-lingual cusp
	2	Most lingual aspect of the anterior-lingual cusp
	3	Most lingual aspect of the metaconid
	4	Most lingual aspect of the entoconid
	5	Most posterior aspect of the posterior cingulum
	6*	Most labial aspect of the posterior labial cusplet
	7	Most labial aspect of the protoconid
	8	Most labial aspect of the anterior-labial cusp
M2	9	Most lingual aspect of the metaconid
	10	Most lingual aspect of the entoconid
	11	Most posterior aspect of the posterior cingulum
	12	Most labial aspect of the protoconid
	13	Most anterior aspect of the anterior labial cusp
M3	14	Most lingual aspect of the metaconid
	15	Most lingual aspect of the entoconid
	16	Most posterior aspect of entoconid (approximately where the enamel meets the root)
	17	Most labial aspect of the protoconid
	18	Most anterior aspect of the anterior-labial cusp

* This landmark is omitted for analyses including all taxa or altered for analyses of larger rats.

Table 3. Description of criteria used to score molar wear stages in the Liang Bua sample. ([back to text](#))

Stage	Description
1	No signs of lamina wearing together Lamina clustered together Auxiliary cusps completely separate High cusps
2	Lamina wearing down Some lamina still higher than others Lamina still separate from one another Auxiliary cusplets showing wear in varying degrees
3	Lamina all largely the same height Lamina still showing distinct curvature for each taxa Lamina starting to wear together Some auxiliary cusplets completely worn into cusps Posterior cingulum still separated from their respective molars
4	Lamina clearly worn together Lamina and molars all similar heights Auxiliary cusplets largely worn into cusps Posterior cingulum showing signs of wearing into their respective molars
5	Little distinction between lamina on each molar Wear between lamina results in "enamal islands" Auxiliary cusplets worn into molars Posterior cingulum worn into their respective molars

Table 4: Descriptions of wear stages as seen in the medium-bodied taxa *Paulamys naso* and *Komodomys rintjanus* as defined for the Liang Bua assemblage. (back to text)

	Paulamys naso	Komodomys rintjanus
Stage 1	M1: Distinctive "heart-shape" present in first lamina; M1: First and second lamina show no signs of wearing together; M1 & M2: Labial and lingual cusps nearly separated with little wear; Auxiliary cusplets present with very little or no wear; Clear separation between lamina in all teeth; High cusps	M1: Lamina distinctly "tucked" together; M1: First and second lamina show no signs of wearing together; M1 & M2: Labial and lingual cusps nearly separated & not worn together; Auxiliary cusplets present with very little or no wear;
Stage 2	M1: distinctive "heart-shape" 1st lamina still largely present; M1: Shows signs of wearing posteriorly but is not worn into M2; Auxiliary cusplets largely unworn – labial cusplets may show signs of wearing into labial cusps; All cusps remain separate from one another while showing light wear	M1: Lamina clustered less tightly together and no longer distinctly "tucked"; M1: Posterolabial cusplet exhibits mild to moderate wear into third lamina; M2: Anterolabial cusplet likely completely or nearly worn into 1st
Stage 3	M1: Distinctive "heart-shape" worn away; M1: Second and third lamina appear closer to same height – distinctive unworn high cusps no longer present; Auxillary labial cusplets beginning so show more wear – likely not all at the same stage; Posterior cingulum still separated from their respective molars; Curvature of lamina still visible	M1: First and second lamina beginning to or almost worn together (typically lingually); M1: Posterolabial cusplet mostly worn into third lamina; M2: Posterolabial cusplet mostly worn into second lamina; Posterior cingulum still separated from their respective molars; Curvature of lamina still visible; All Lamina still largely separate
Stage 4	M1: Shows wear between first and second lamina – severity will vary but they likely will not be completely worn together (wear will be central or slightly lingual); Most auxiliary cusplets are largely worn in including anterocentral cusplet on M2; All molars and lamina now largely the same height; Posterior cingulum may or may not still be separated	M1: First and second lamina worn together (typically lingually); All auxiliary cusplets worn into main cusps; Lamina showing signs of losing their distinctive curved shape; Posterior cingulum show signs of wearing into lamina; Lamina begin wearing together via auxiliary cusplets – overall shape of molar becomes obfuscated
Stage 5	Lamina within each molar almost completely worn together both labially and lingually; Posterior cingulum worn into lamina; All lamina appear to be largely the same height; "Islands" may be present in centre of teeth with lamina may not yet have fully worn together; M3 shows considerable wear; Original shape of toothrow largely lost	

Table 5. Descriptions of wear stages as seen in *Papagomys armandvillei*. ([back to text](#))

Stage	Description
1	Lamina show no signs of wear High cusps Lamina appear to be "chevron in shape" (Musser, 1981)
2	Largely unworn or showing slight wear to occlusal surface Auxiliary cusps (if present) likely unworn of showing very minimal signs of wear Labial and lingual cusps largely separate with little wear between the two (this will vary) Posterior cingulum remains distinctly separate from lamina
3	Medium to moderate wear to occlusal surface Auxiliary cusps (if present) show significant signs of wear into main cusps Labial and lingual cusps no longer completely distinct, though some separation may still be present "Chevron" shape of lamina largely worn away and no longer distinctive Lamina may show signs of wearing together Posterior cingulum showing signs of wear into the posterior aspect of their respective molars, wear likely beginning around the labial and lingual margins of the posterior cingulum
4	Occlusal surface largely worn Auxiliary cusps (if present) nearly completely worn into main cusps Labial and lingual cusps no longer separate and appear are one large lamina "Chevron" shape of lamina completely worn away and no longer discernable Lamina likely to show signs of wearing together both in the midline of the tooth and around the occlusal outline (severity will vary) Posterior cingulum completely or nearly completely worn into posterior aspect of their respective molars
5	Occlusal surface completely worn Auxiliary cusps (if present) completely worn into main cusps "enamal islands" likely present

Table 6. Breakdown of the taxonomic identifications for the Liang Bua archaeological sample based on the 2DGM results of this study. (back to text)

Taxa	Number of Specimens
Papagomys armandvillei	13
Papagomys theodorverhoeveni	7
Spelaeomys florensis	4
Hooijeromys cf. *nusatenggara*	12
Paulamys naso	39
Komodomys rintjanus	62
small *Rattus* sp.	20

Figures
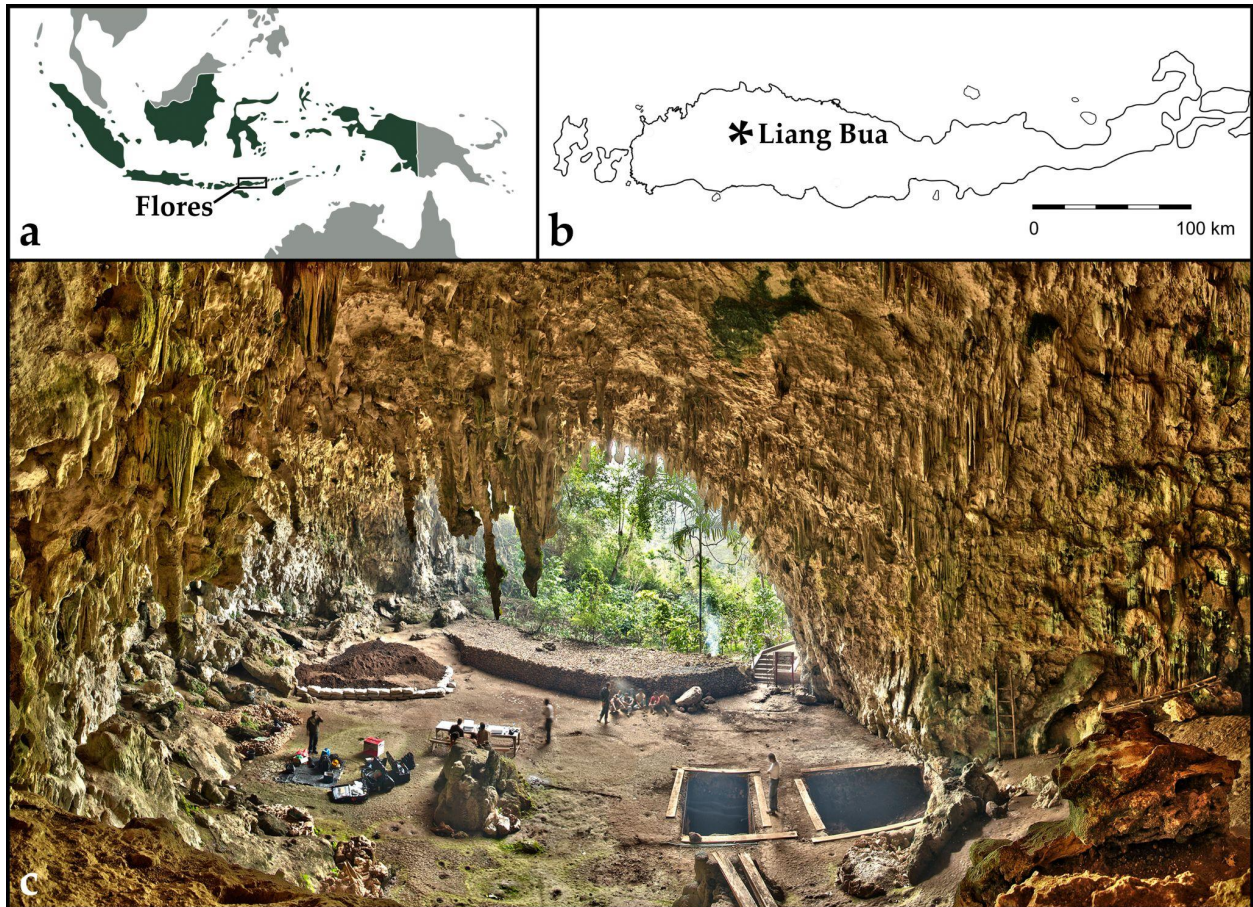
Figure 1. The geographic location of Flores within Indonesia (a), the location of Liang Bua on Flores (b), and a map of the site (c). Cave floor sediments are shaded white, while the shaded areas are exposed rocks, stalagmites and other surfaces covered in speleothems (a and b, modified from Sutikna et al., 2016; and c, courtesy of Smithsonian 3d.si.edu/Liang Bua Team). (back to text)
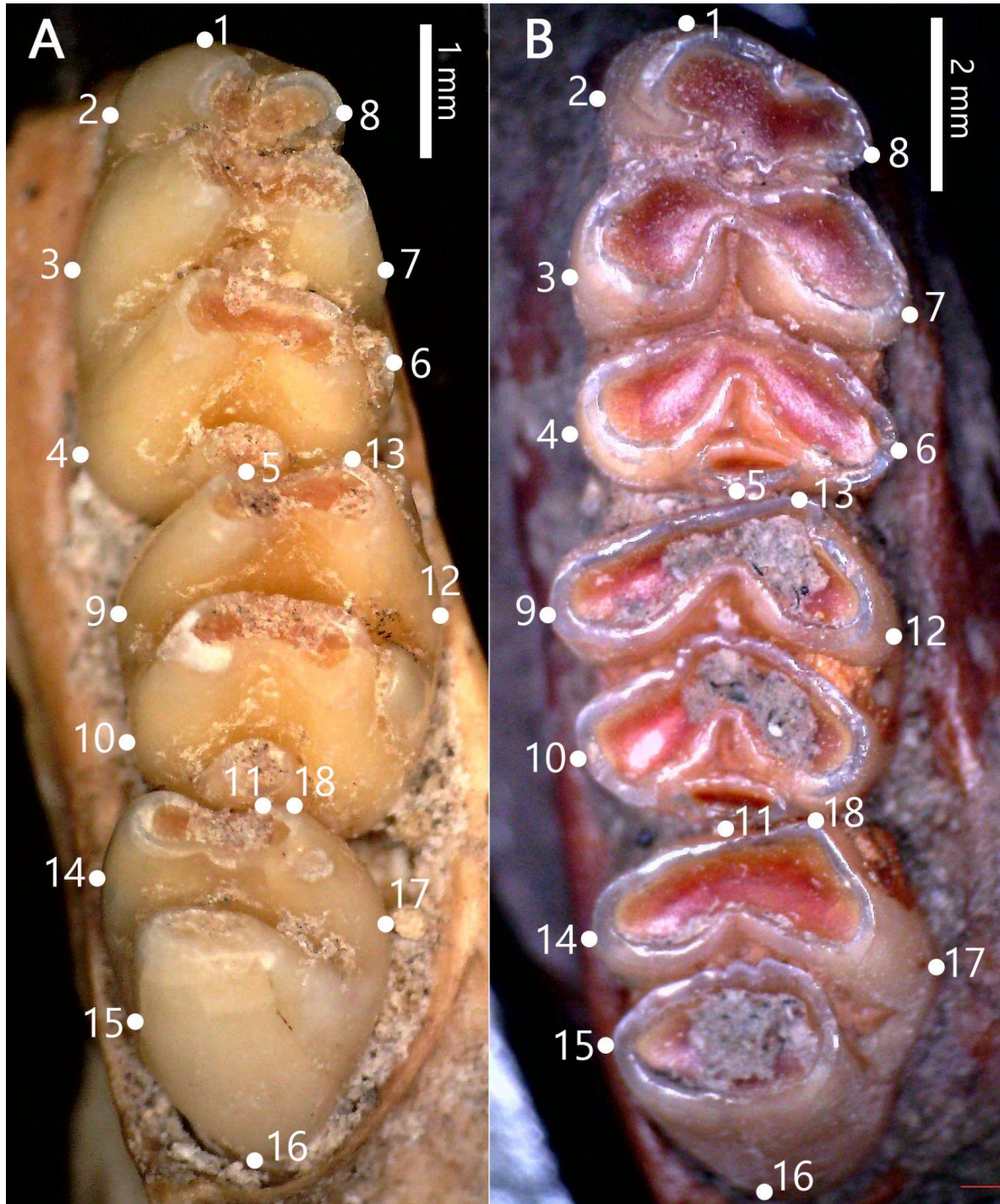
Figure 2. The landmarks used in this study. (A) 18 landmarks included eight landmarks on the first molar (#1–8), five on the second molar (#9–13), and five on the third molar (#14–18). The right mandibular molars of a *Paulamys naso* specimen from Liang Bua are shown. For some analyses, landmark #6 was omitted, or as shown in (B), modified slightly (see text for details). The right mandibular molars of *Papagomys armandvillei* are shown. ([back to text](#))

Figure 3. Examples of the five molar wear stages (from left to right, from least to most worn) observed in the medium-sized rats from Liang Bua. (back to text)

Figure 4. Examples of the three molar wear stages (from left to right, stages 2, 3, and 4) observed in the *Papagomys armandvillei* sample. Note wear stages 1 and 5 were not observed in this study. (back to text)
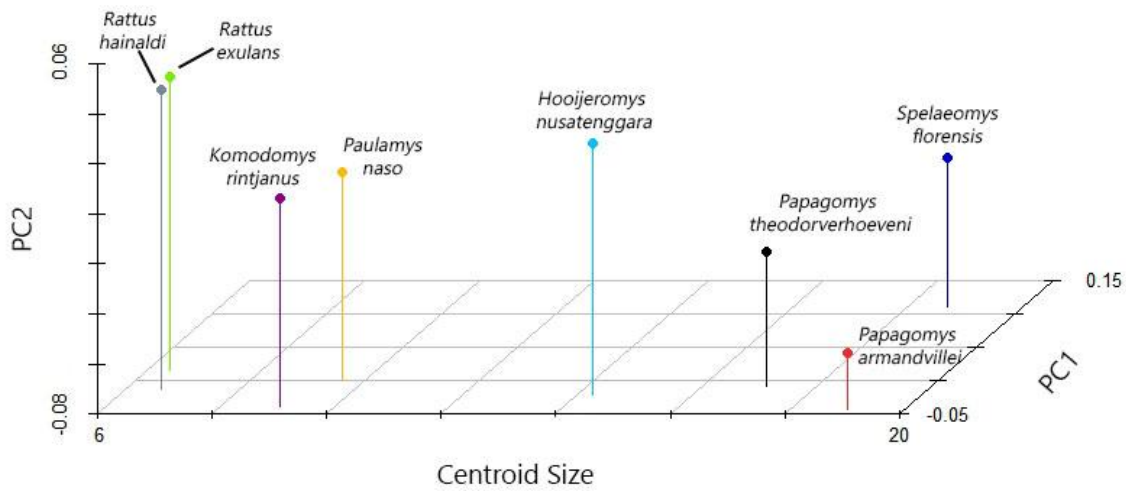
Figure 5A. Shape and size analysis results of the 2DGM comparisons of the holotypes or reasonable substitutes of the endemic rats of Flores. Plot of PC1 and PC2 against centroid size. The centroid size axis shows clear differentiation among the different size classes while PC1 and PC2 show separation of comparably sized taxa (e.g., *Paulamys naso* versus *Komodomys rintjanus*). (back to text)
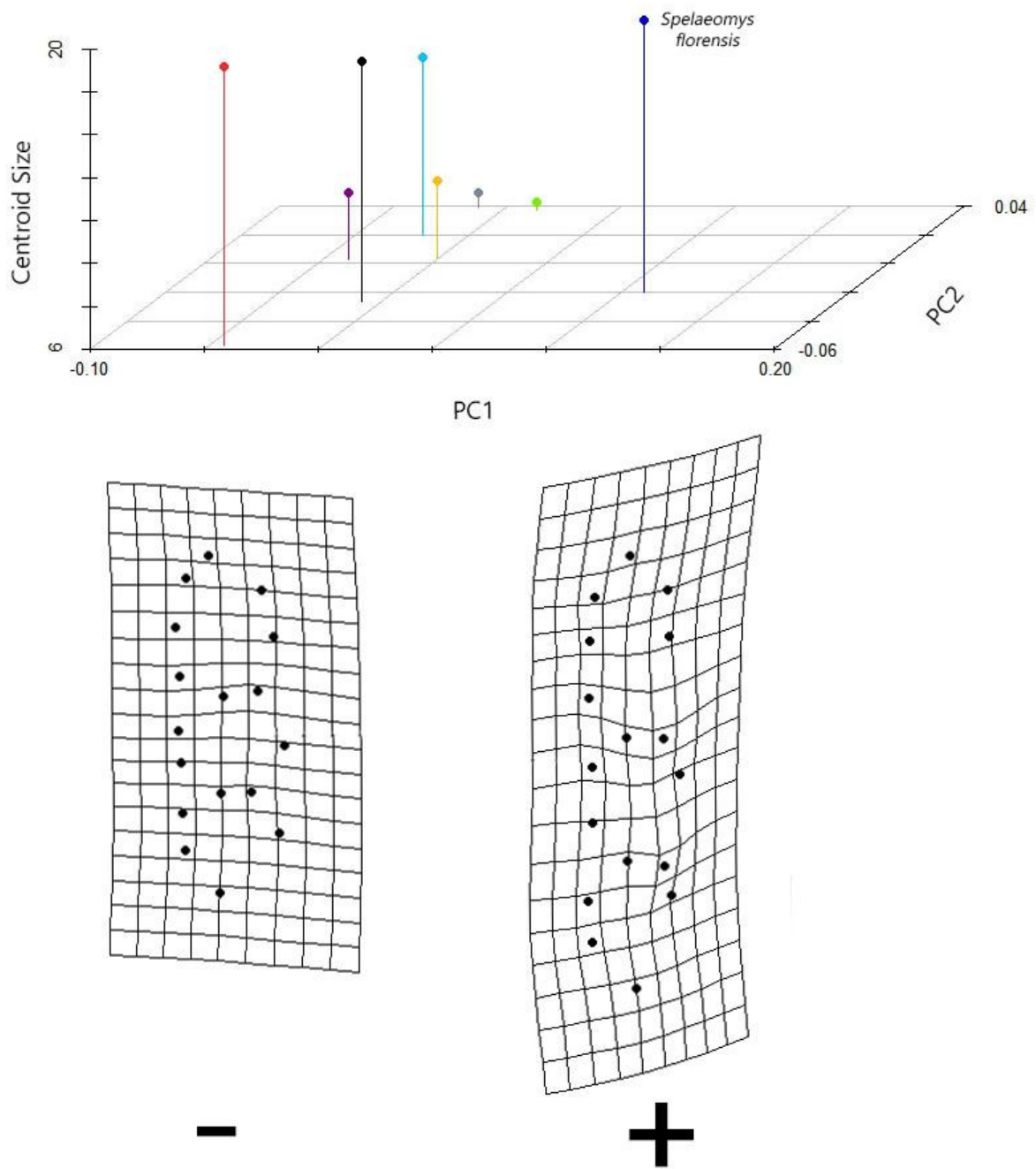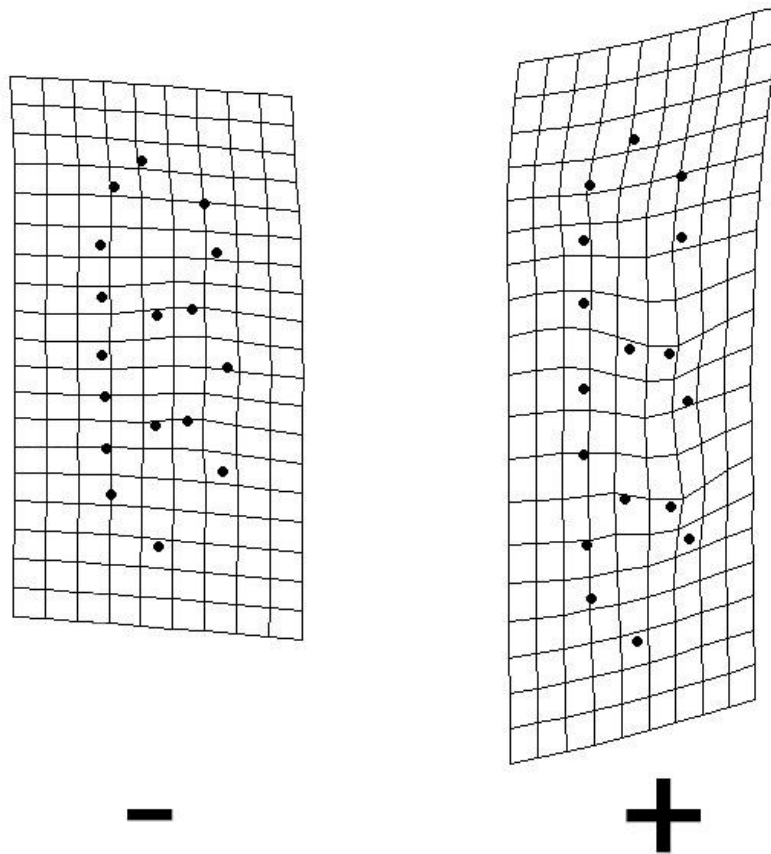
Figure 5B. Plot of PC2 and centroid size against PC1 with thin plate splines showing the shapes of the extreme specimens along PC1. (back to text)
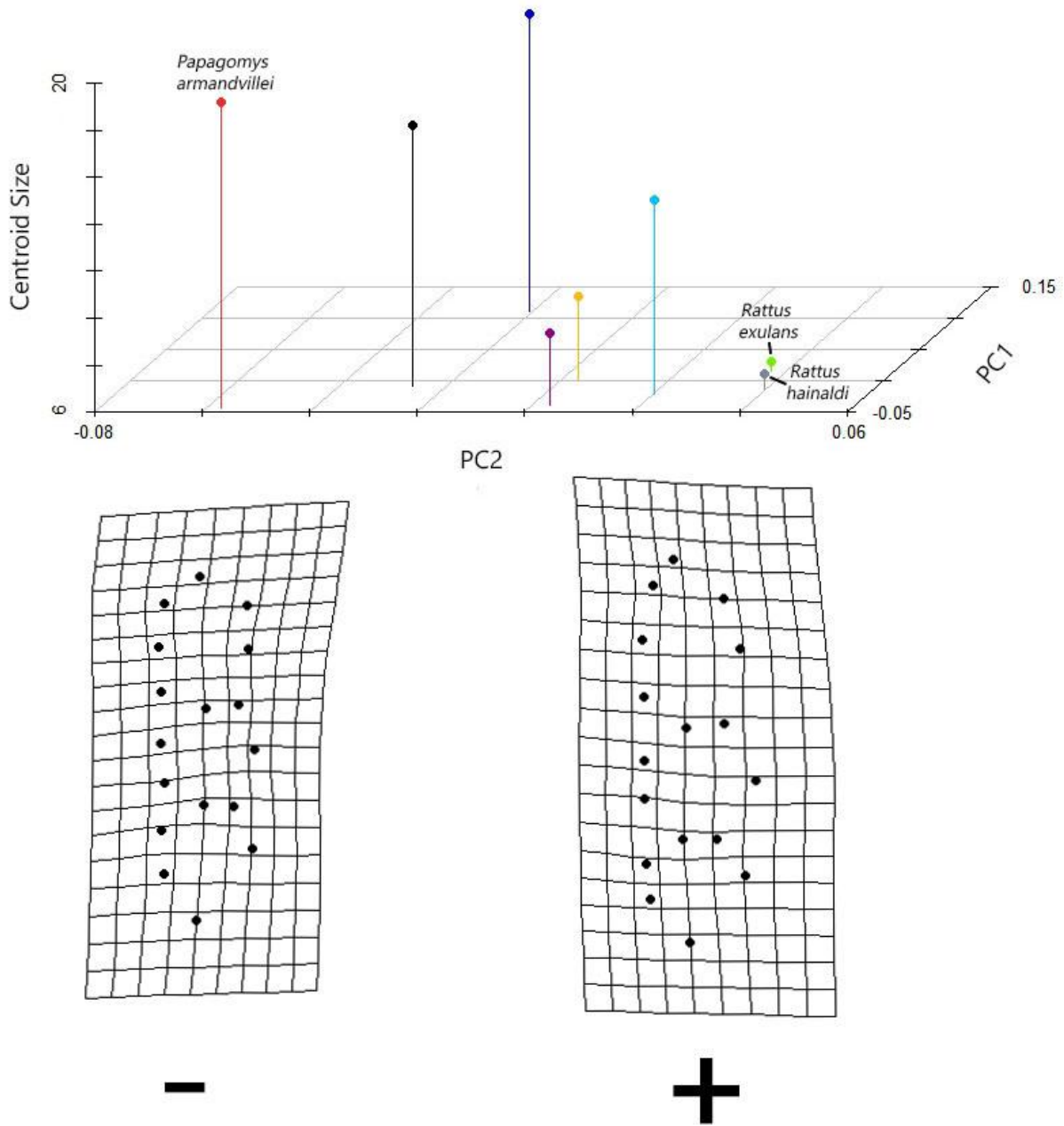
Figure 5C. Plot of PC1 and centroid size against PC2 with thin plate splines showing the shapes of the extreme specimens along PC2. (back to text)
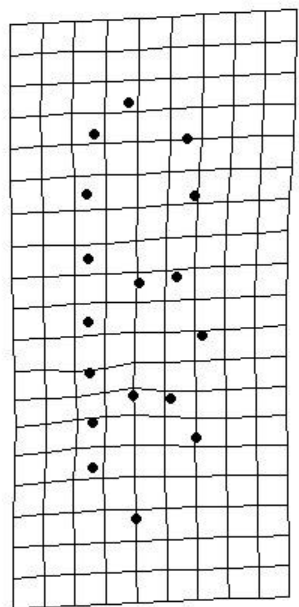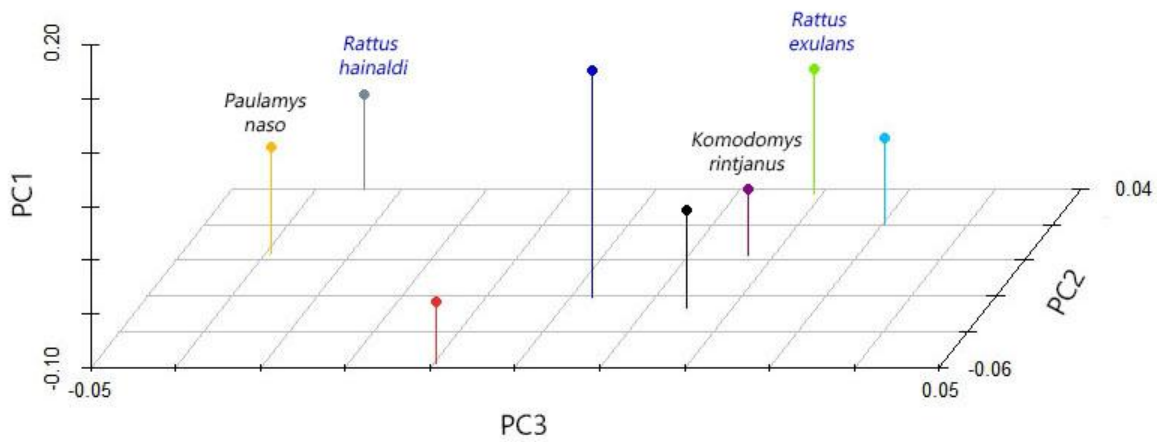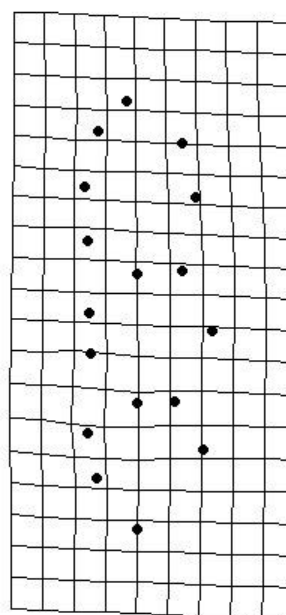
Figure 5D. Plot of PC2 and PC1 against PC3 with thin plate splines showing the shapes of the extreme specimens along PC3. (back to text)

Figure 6. Right mandibular molar row of *Spelaeomys florensis* from Liang Bua. Note the multiple auxiliary cusplets on the labial side of the first and second molars. (back to text)
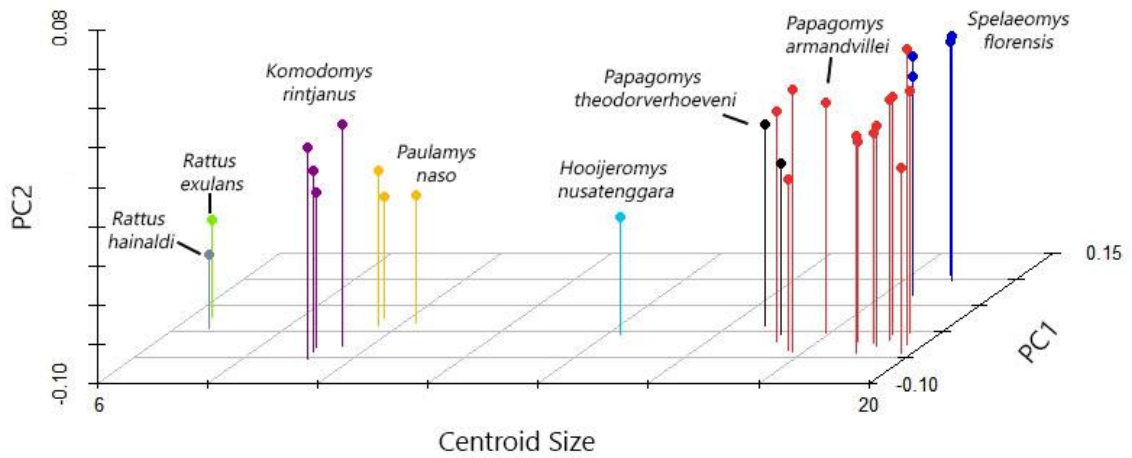
Figure 7A. Shape and size analysis results of the comparisons of the confirmed specimens of the endemic rats of Flores. Plot of PC1 and PC2 against centroid size. The centroid size axis shows clear differentiation among the different size classes while PC1 and PC2 show separation of comparably sized taxa (e.g., *Paulamys naso* versus *Komodomys rintjanus*). (back to text)
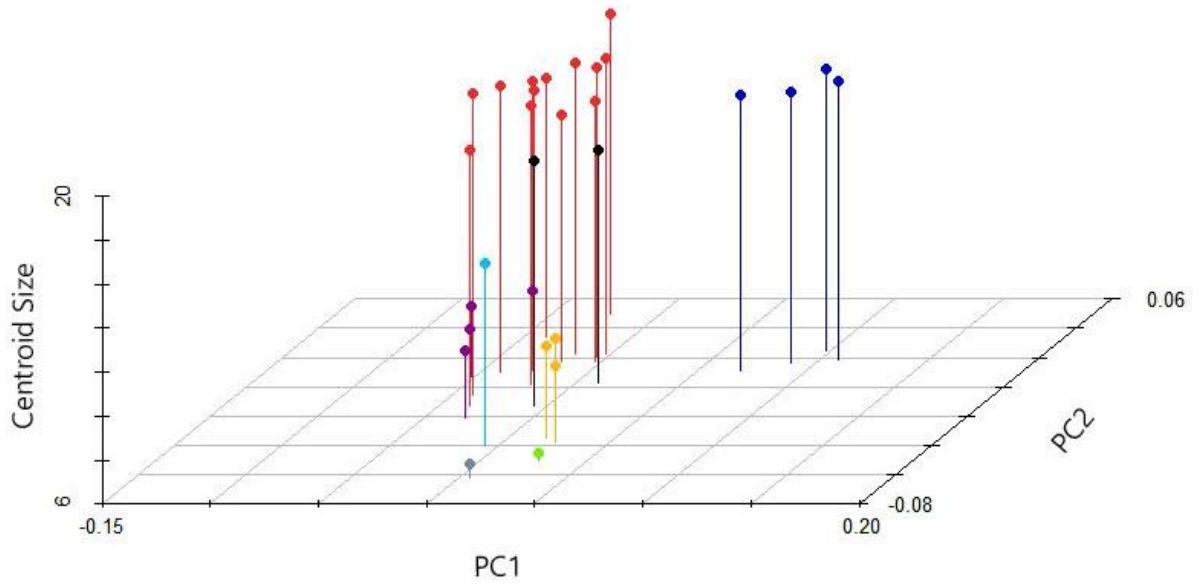
Figure 7B. Plot of PC2 and centroid size against PC1 with thin plate splines showing the shapes of the extreme specimens along PC1. (back to text)
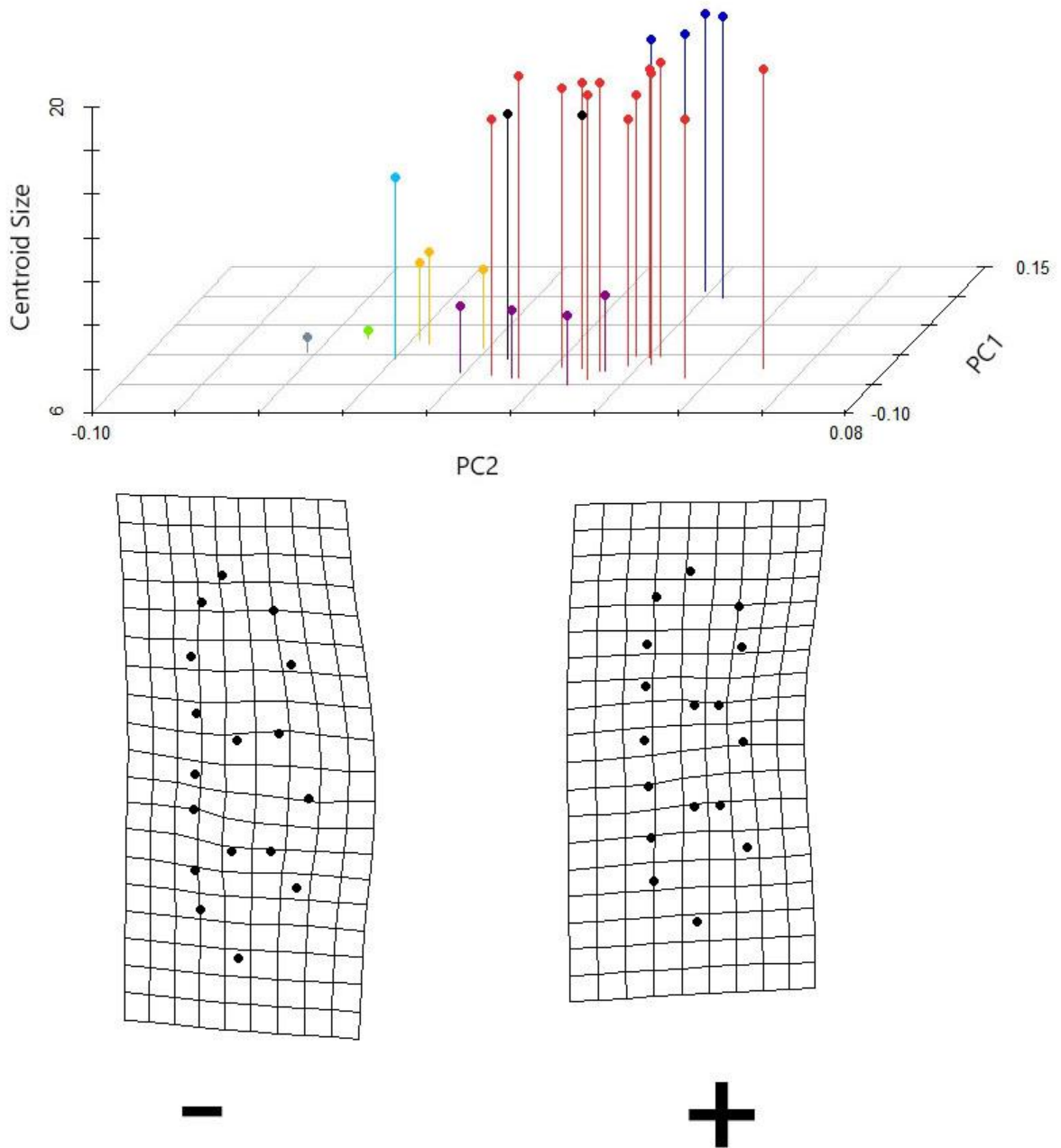
Figure 7C. Plot of PC1 and centroid size against PC2 with thin plate splines showing the shapes of the extreme specimens along PC2. (back to text).
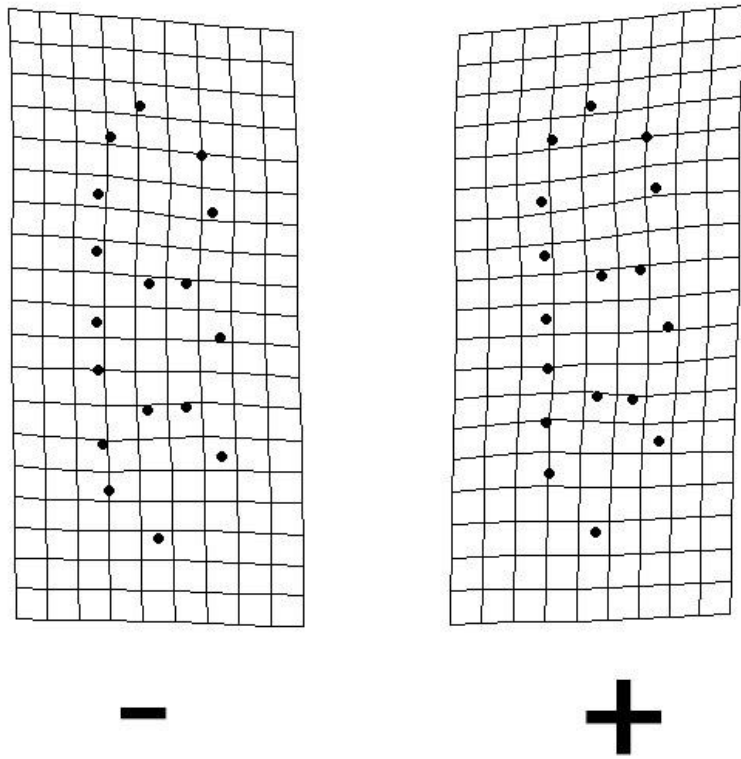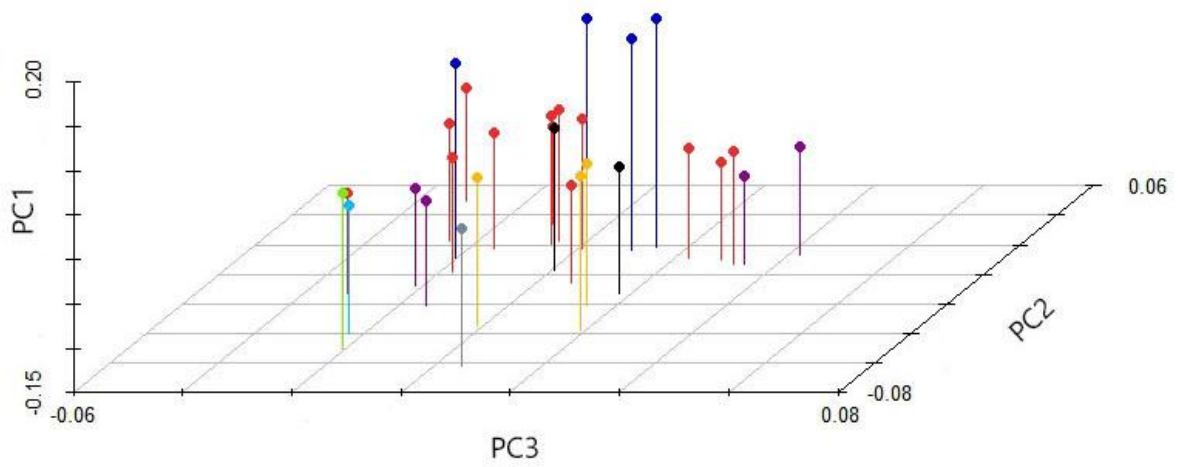
Figure 7D. Plot of PC2 and PC1 against PC3 with thin plate splines showing the shapes of the extreme specimens along PC3. (back to text)

Figure 8A. Plot of PC1 and PC2 showing the *Rattus hainaldi* (light grey), *Rattus exulans* (green), and small *Rattus* sp. (purple) with thin plate splines showing the shapes of the extreme specimens along PC1. Holotypes are indicated by the large stars. (back to text)
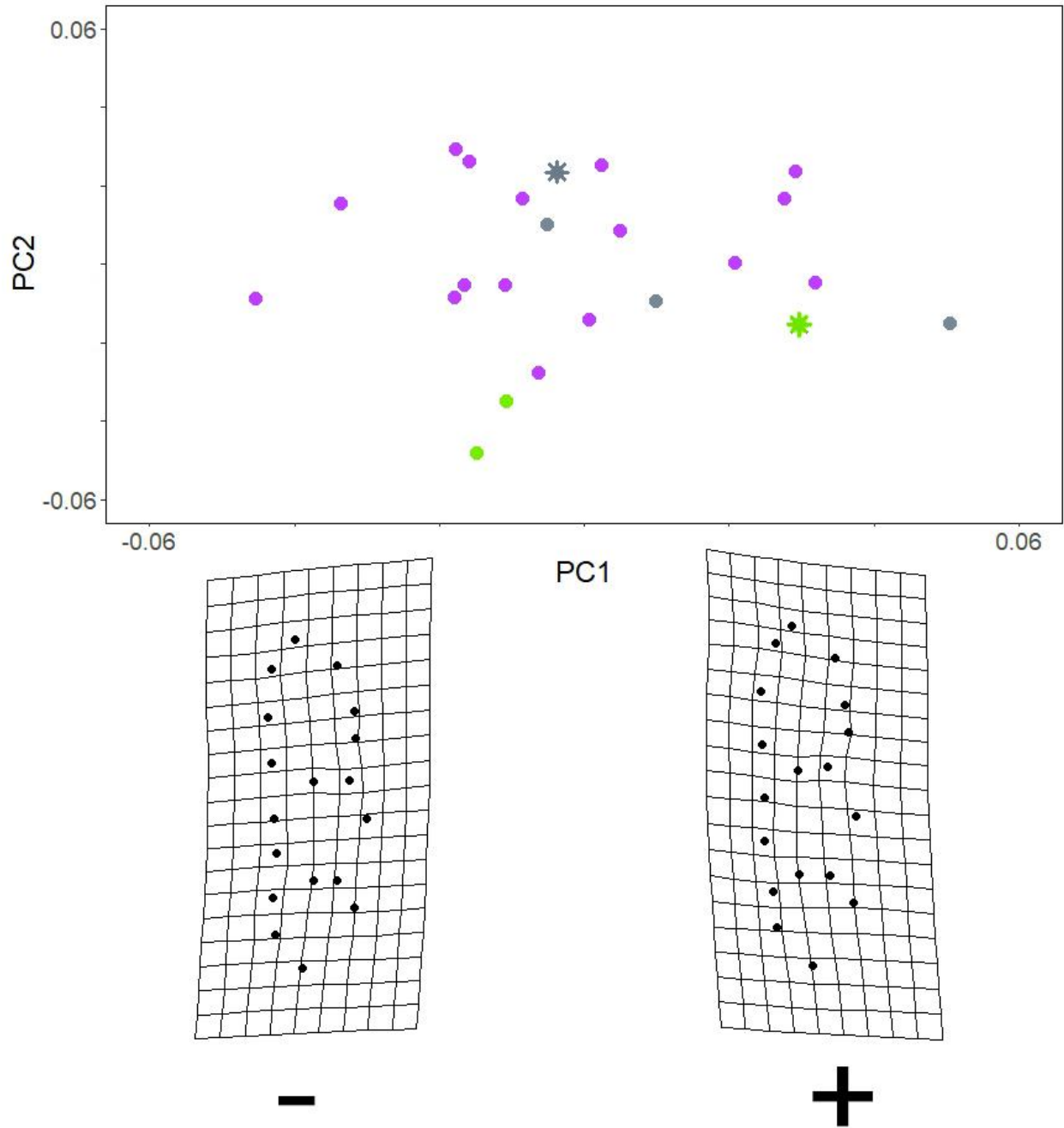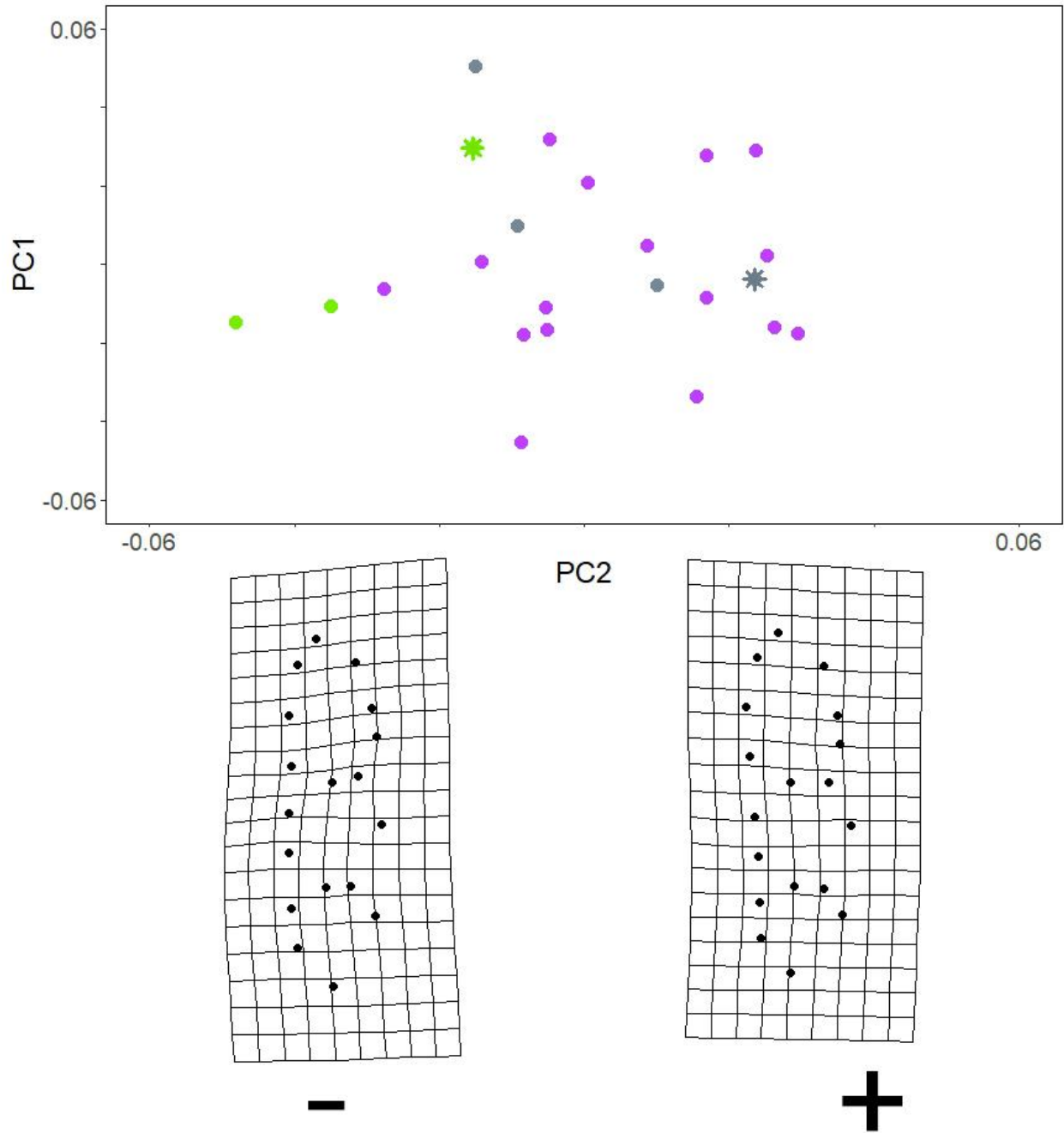
Figure 8B. Plot of PC2 and PC1 showing the *Rattus hainaldi* (light grey), *Rattus exulans* (green), and small *Rattus* sp. (purple) with thin plate splines showing the shapes of the extreme specimens along PC2. Holotypes are indicated by the large stars. (back to text)

Figure 9A. Plot of PC1 and PC2 showing the *Paulamys naso* (yellow) and *Komodomys rintjanus* (purple) with thin plate splines showing the shapes of the extreme specimens along PC1. Holotypes are indicated by the large stars and confirmed specimens are indicated by the smaller stars. ([back to text](#))
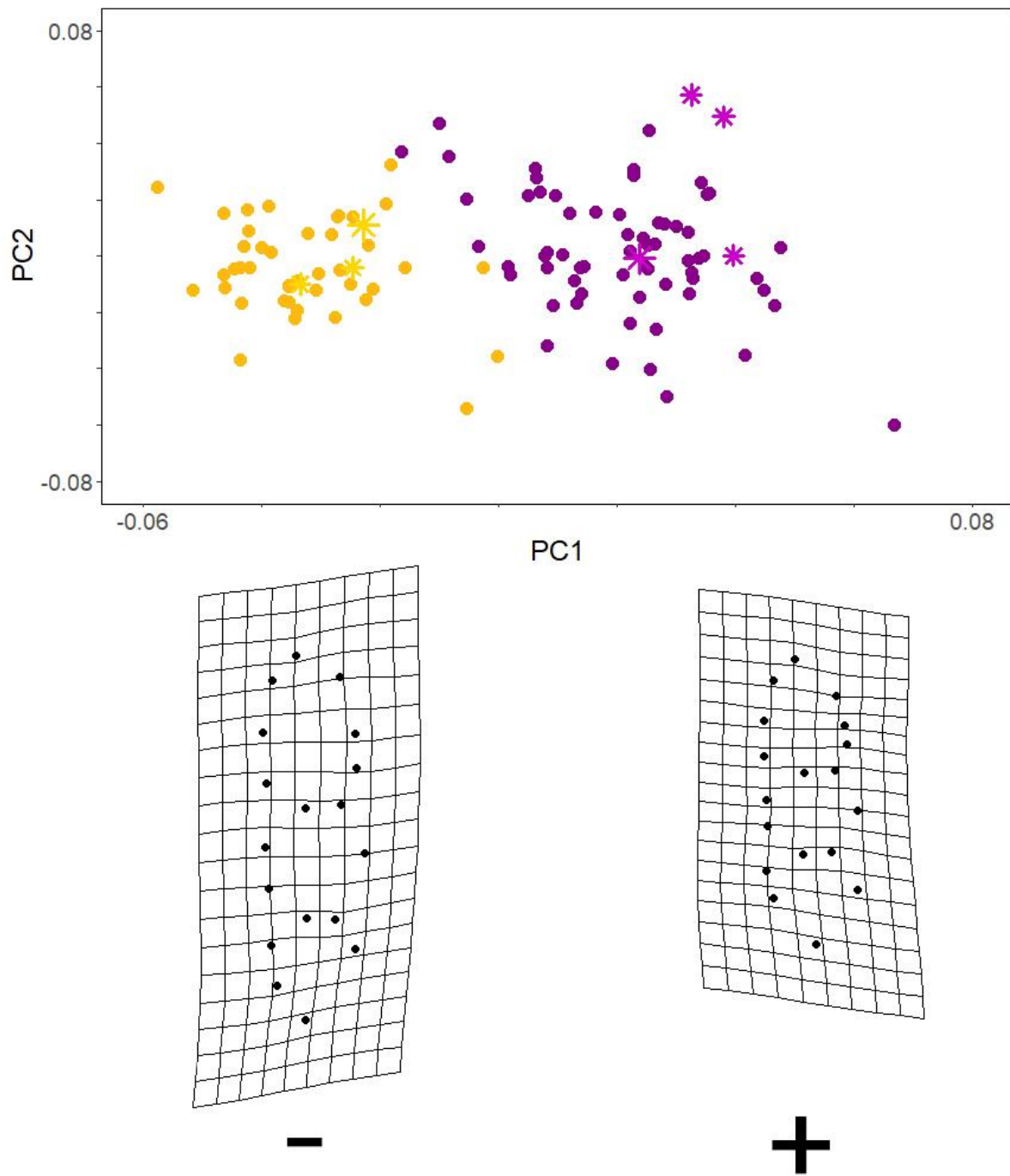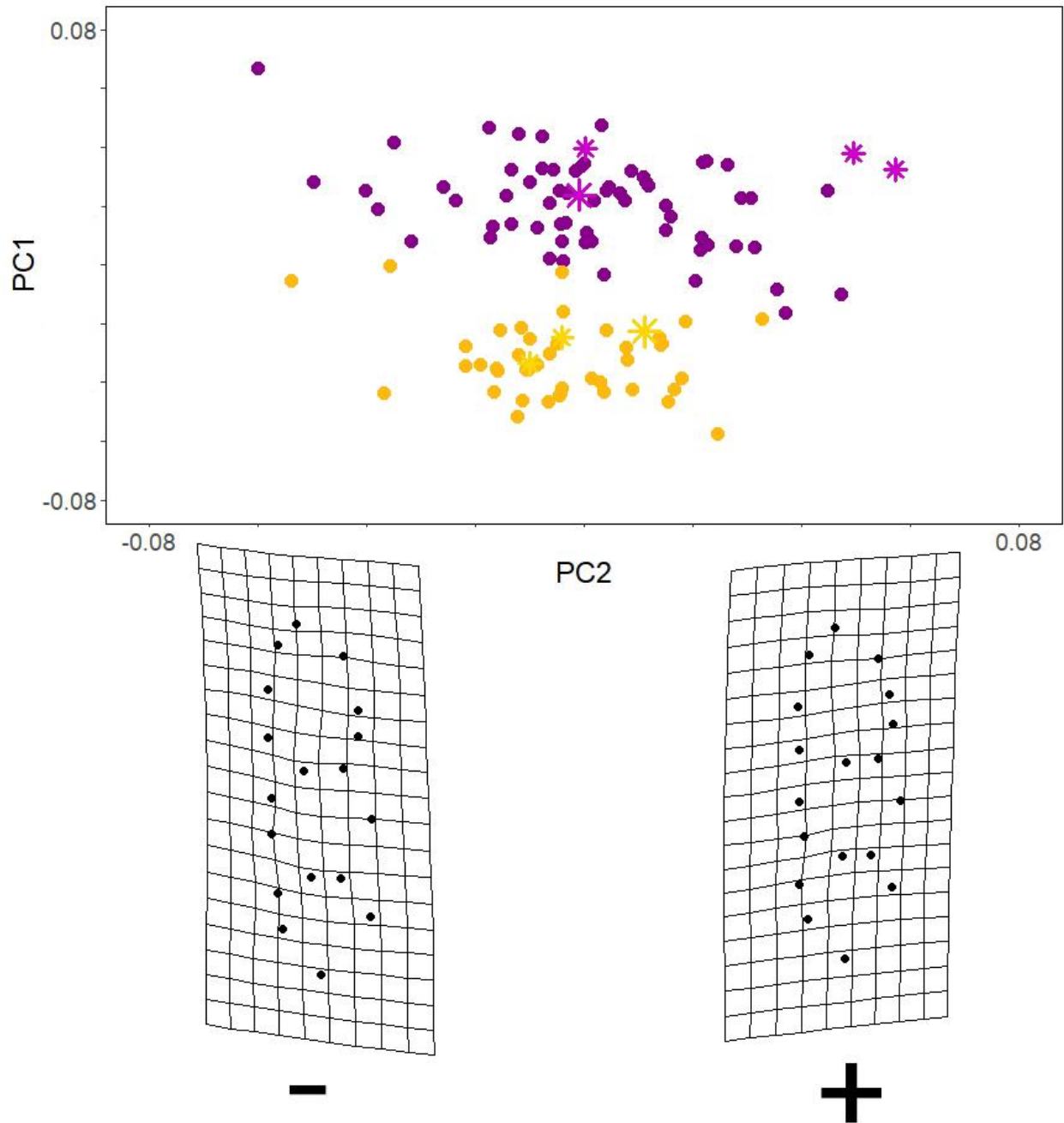
Figure 9B. Plot of PC1 and PC2 showing the *Paulamys naso* (yellow) and *Komodomys rintjanus* (purple) with thin plate splines showing the shapes of the extreme specimens along PC1. Holotypes are indicated by the large stars and confirmed specimens are indicated by the smaller stars. ([back to text](#))
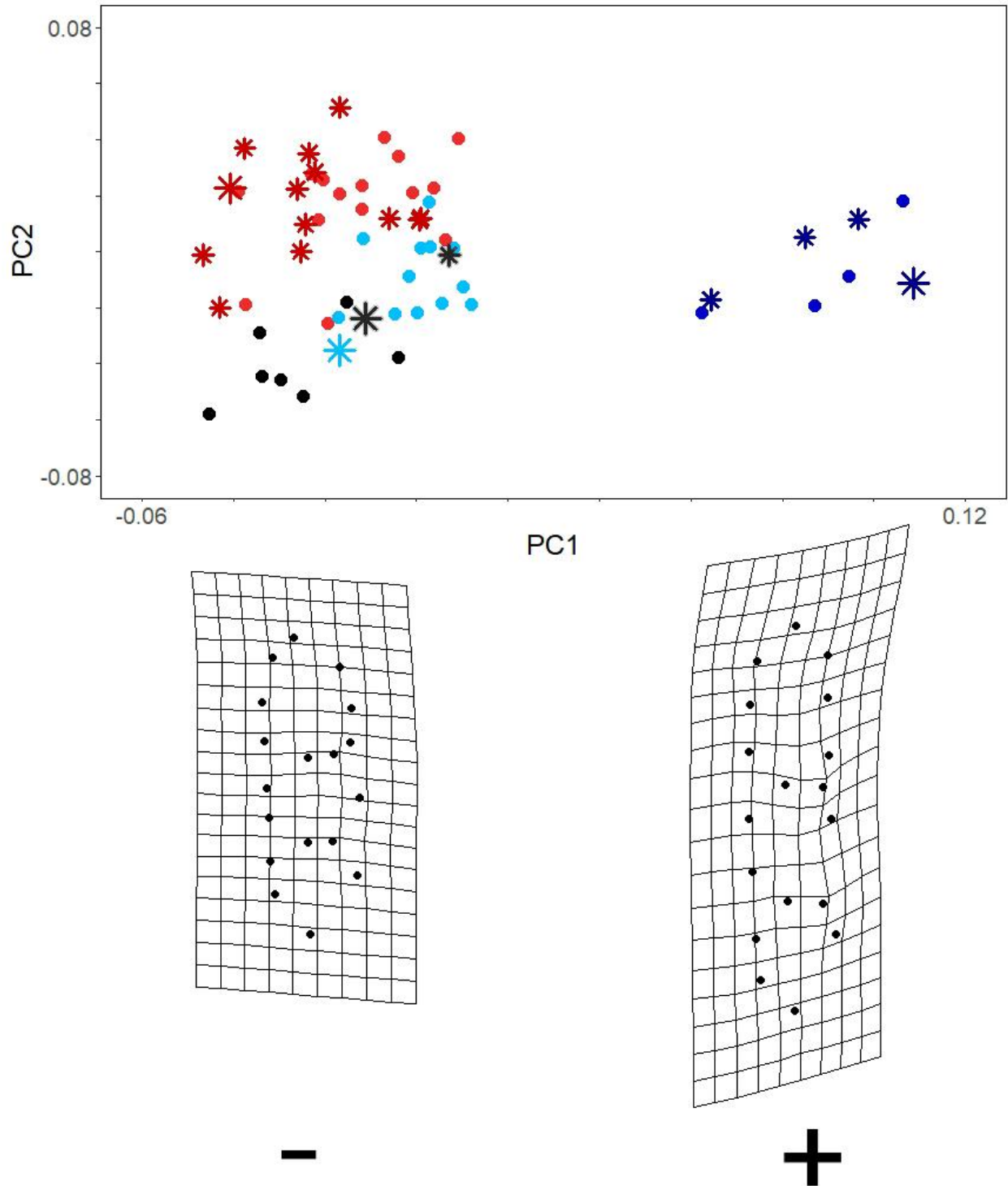
Figure 10A. Plot of PC2 and PC1 showing the larger-sized taxa with thin plate splines showing the shapes of the extreme specimens along PC2. Holotypes are indicated by the large stars and confirmed specimens are indicated by the smaller stars. (back to text)
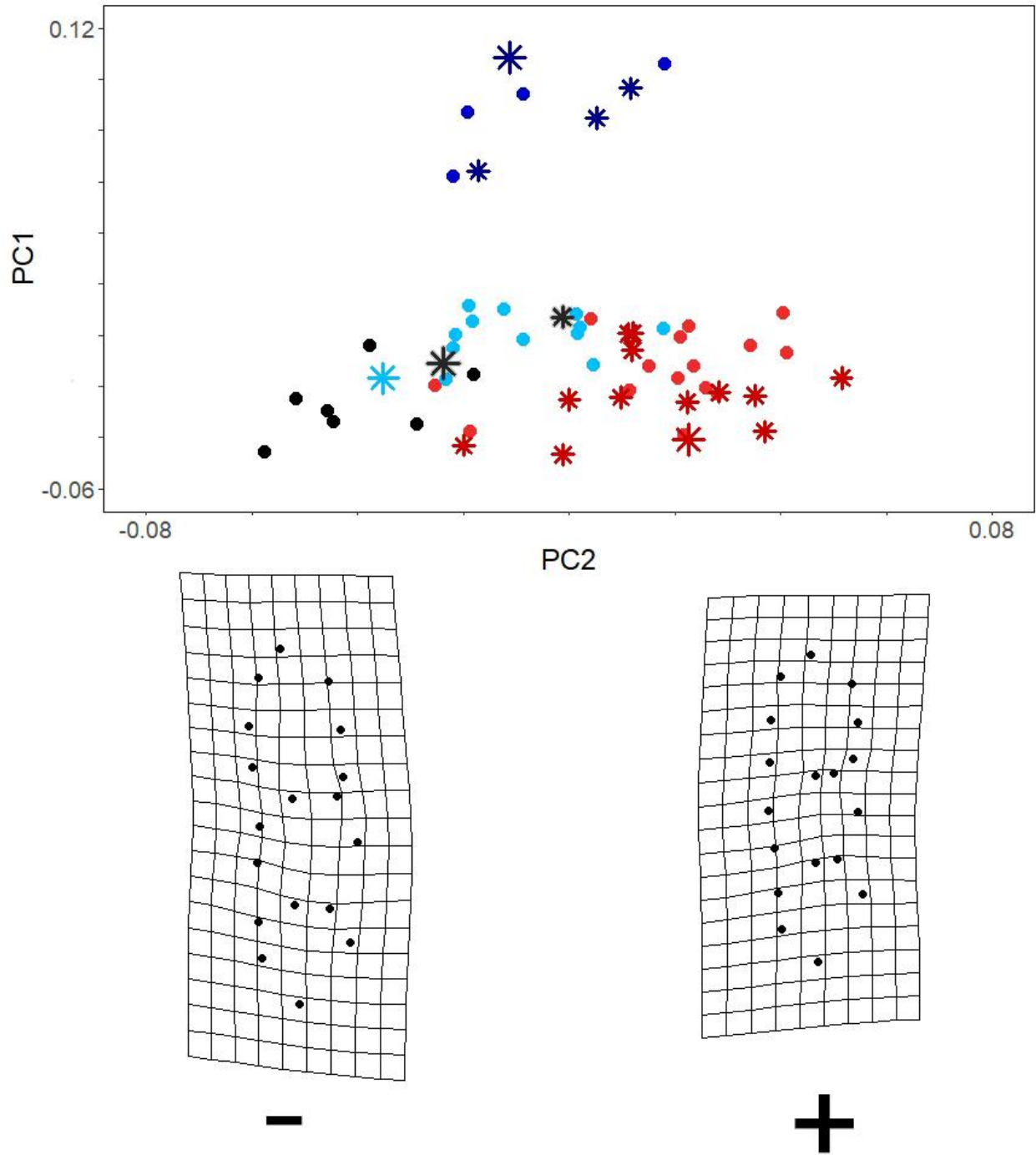
Figure 10B. Plot of PC2 and PC1 with thin plate splines showing the shapes of the extreme specimens along PC2. Holotypes are indicated by the large stars and confirmed specimens are indicated by the smaller stars. (back to text)
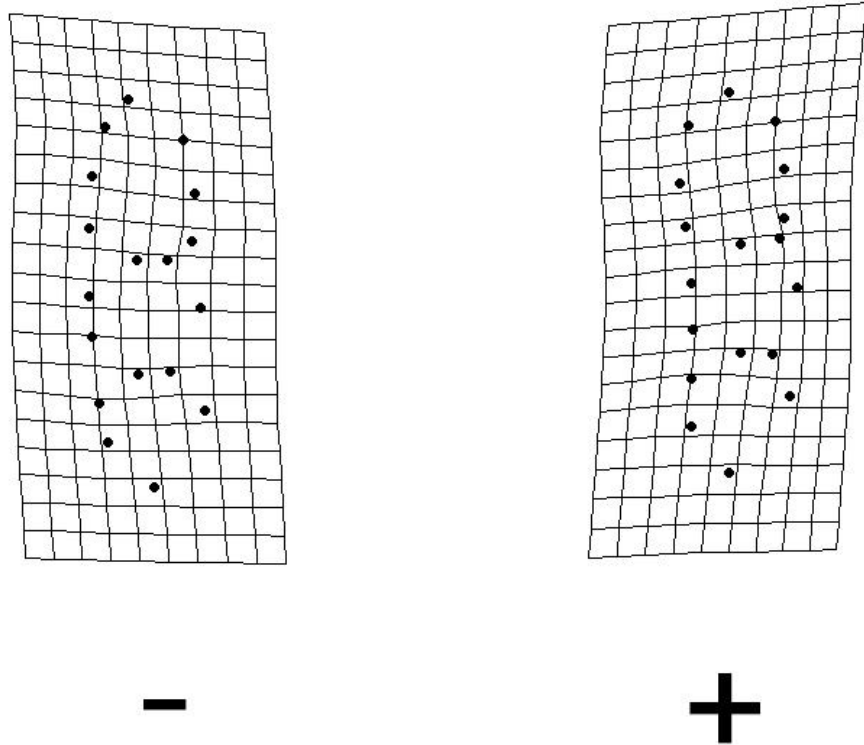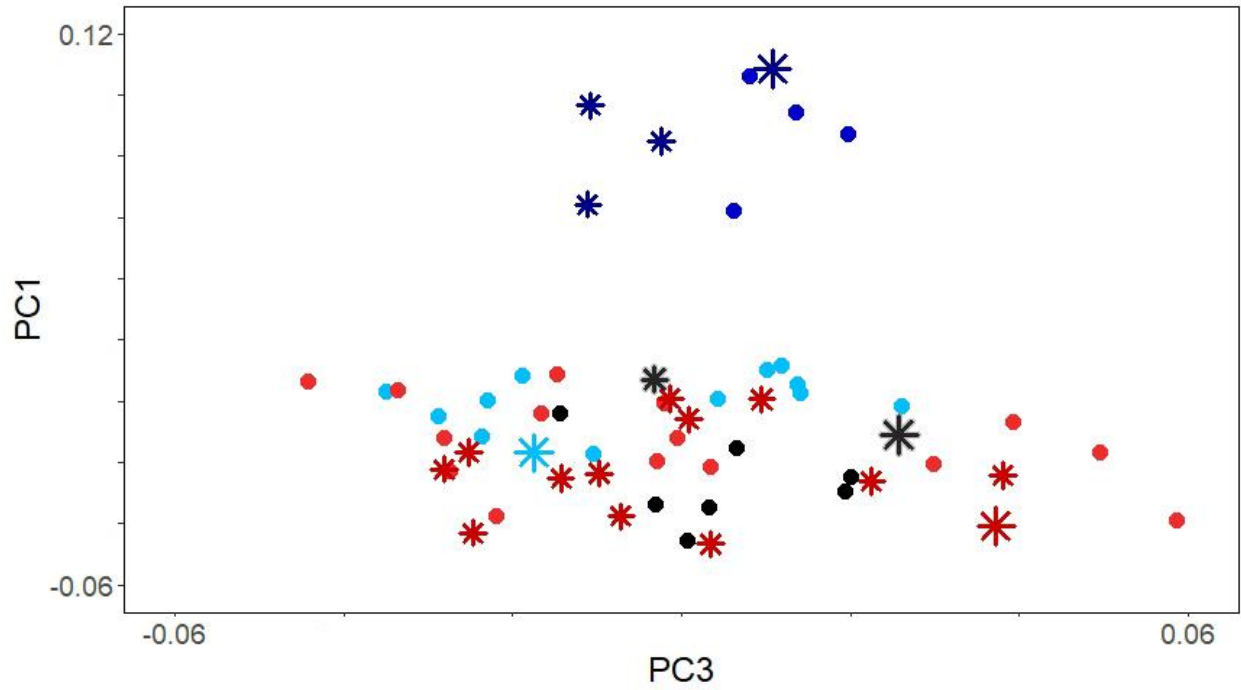
Figure 10C. Plot of PC3 and PC1 with thin plate splines showing the shapes of the extreme specimens along PC3. Holotypes are indicated by the large stars and confirmed specimens are indicated by the smaller stars. (Back to text)
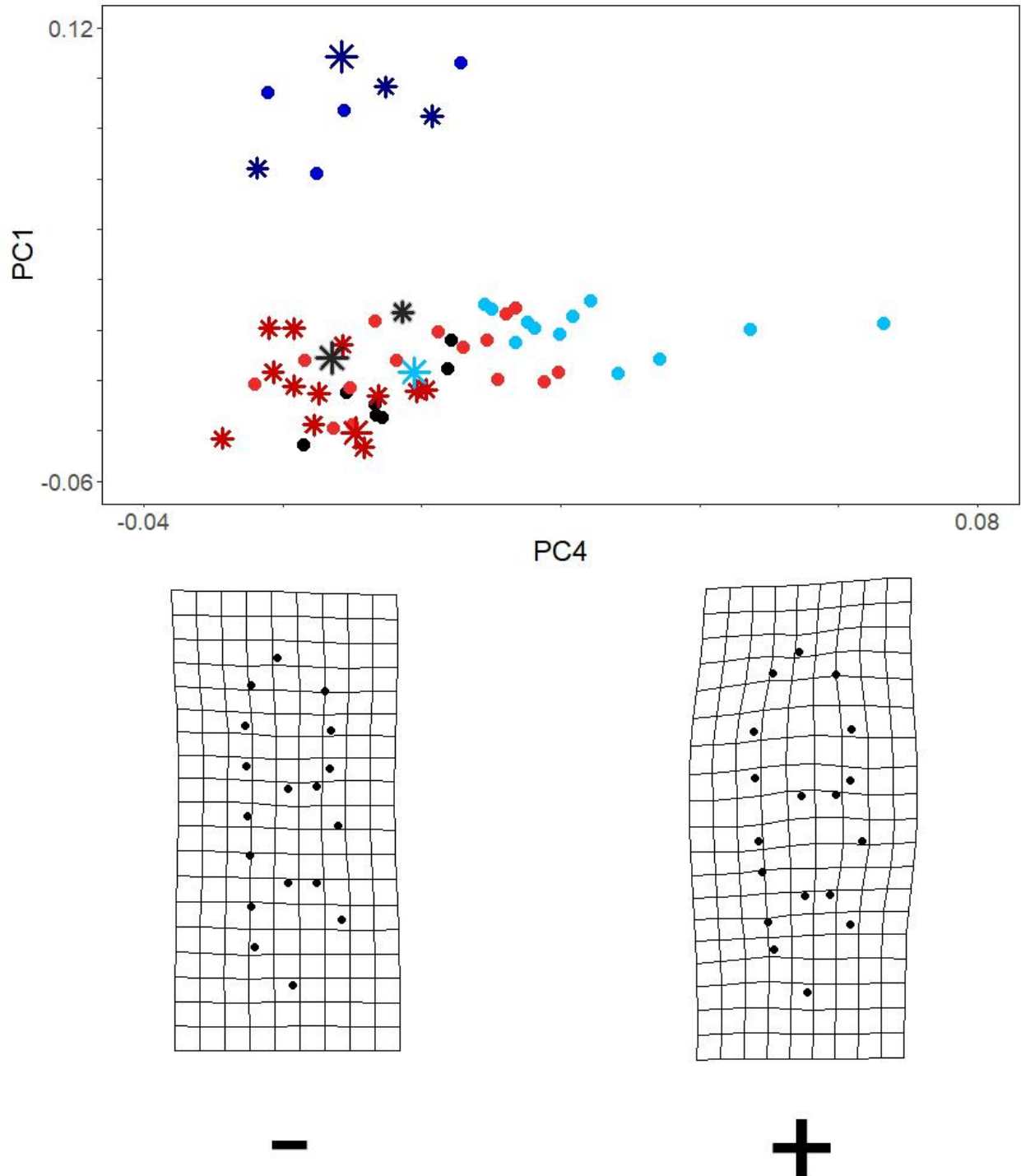
Figure 10D. Plot of PC4 and PC1 with thin plate splines showing the shapes of the extreme specimens along PC4. Holotypes are indicated by the large stars and confirmed specimens are indicated by the smaller stars. (back to text)

| Occlusal | Anterior | Posterior | Lingual | Buccal |

Figure 11. Examples of the five different viewing angles for a single specimen of *Komodomys rintjanus*. (back to text)
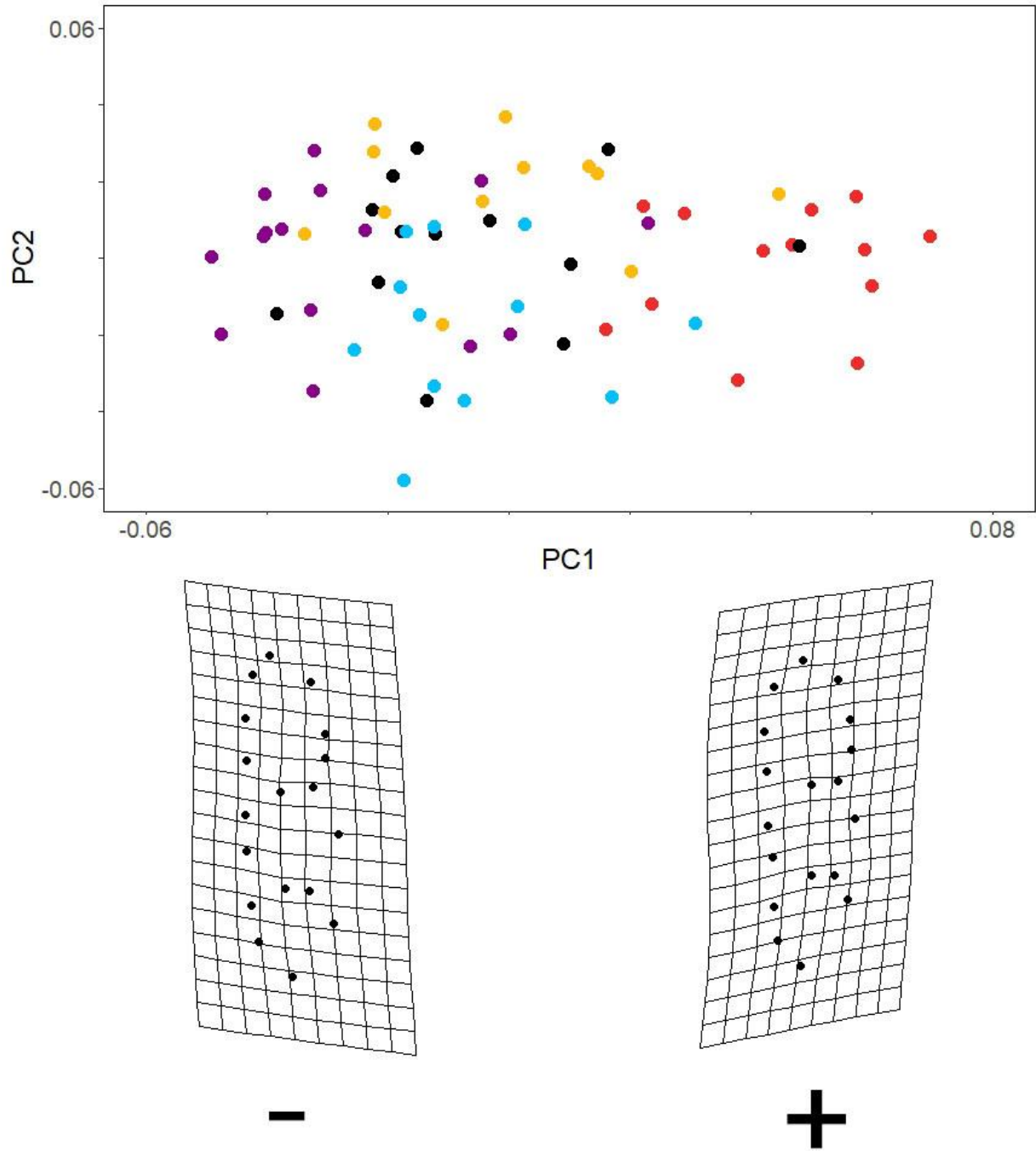
Figure 12A. Plot of PC1 and PC2 showing the shape differences between image viewing angles (purple = buccal; yellow = posterior; black = occlusal; blue = anterior; red = lingual) in *Paulamys naso*. ([back to text](#))
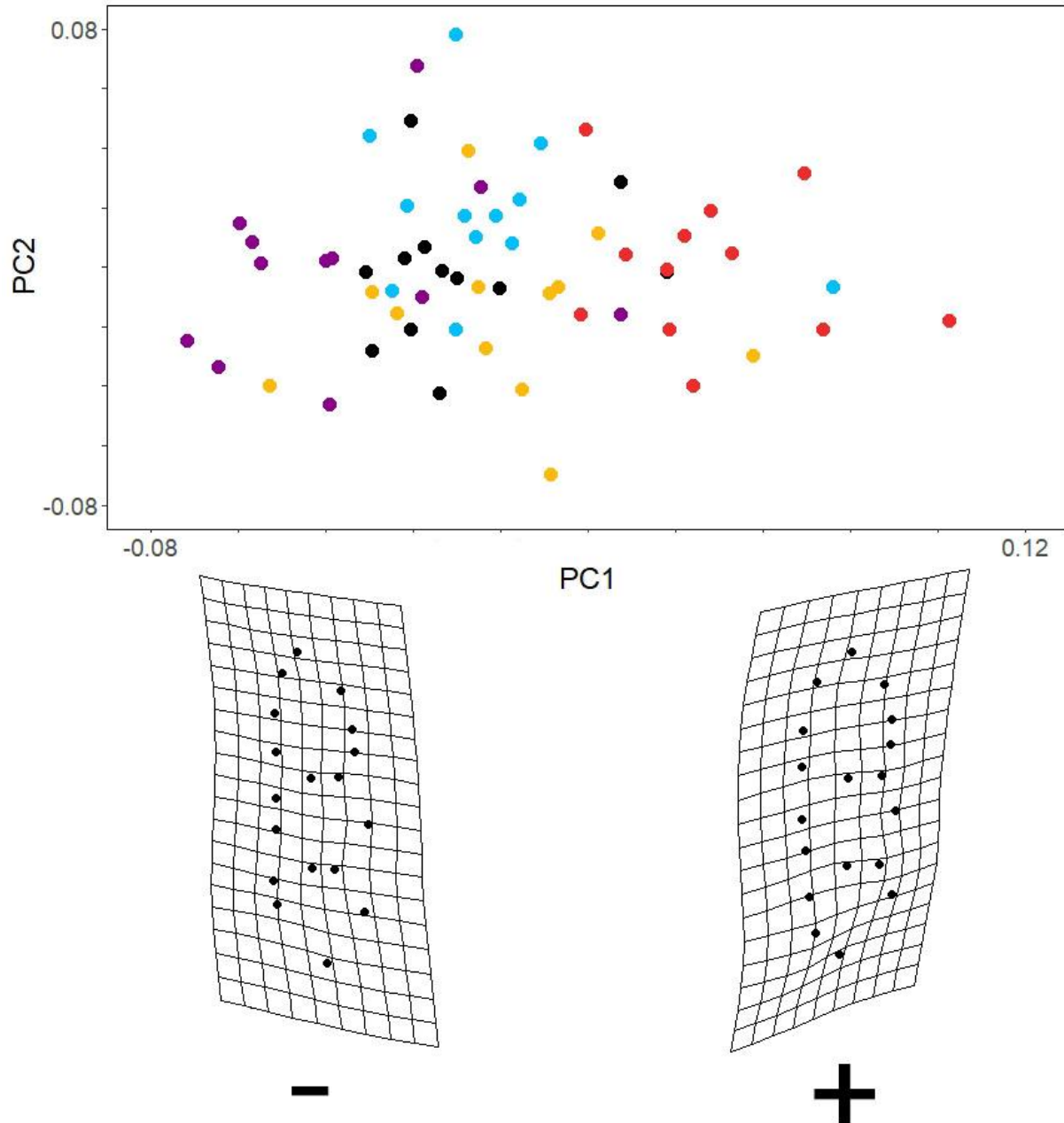
Figure 12B. Plot of PC1 and PC2 showing the shape differences in image viewing angles (purple = buccal; yellow = posterior; black = occlusal; blue = anterior; red = lingual) in *Komodomys rintjanus*. (back to text)
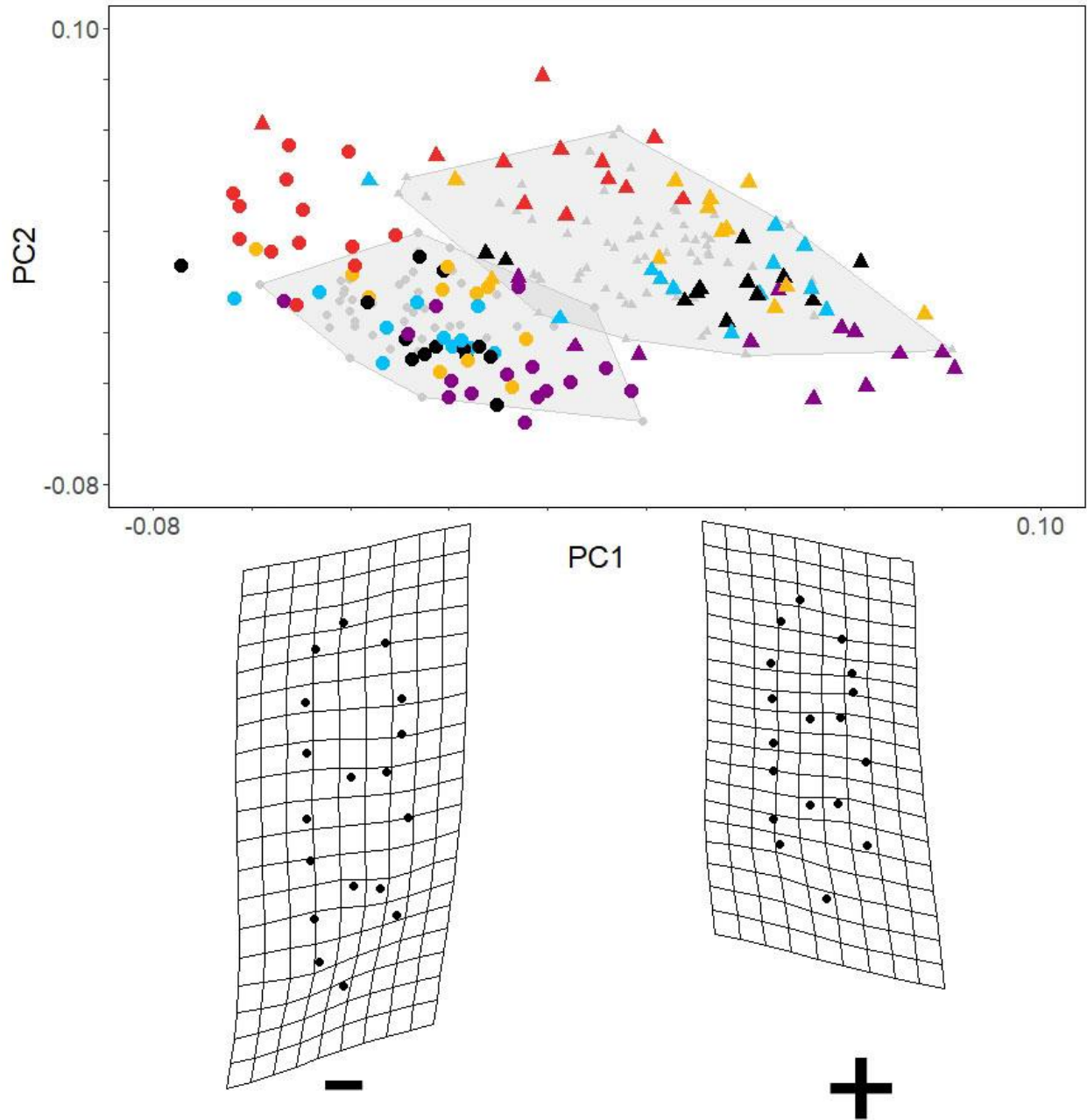
Figure 12C. Plot of PC1 and PC2 showing the different image angles (red = lingual; yellow = posterior; black = occlusal; blue = anterior; purple = buccal) in *Paulamys naso* (circles) and *Komodomys rintjanus* (triangles). Grey convex hulls represent the total archaeological sample used in this study. ([back to text](#))
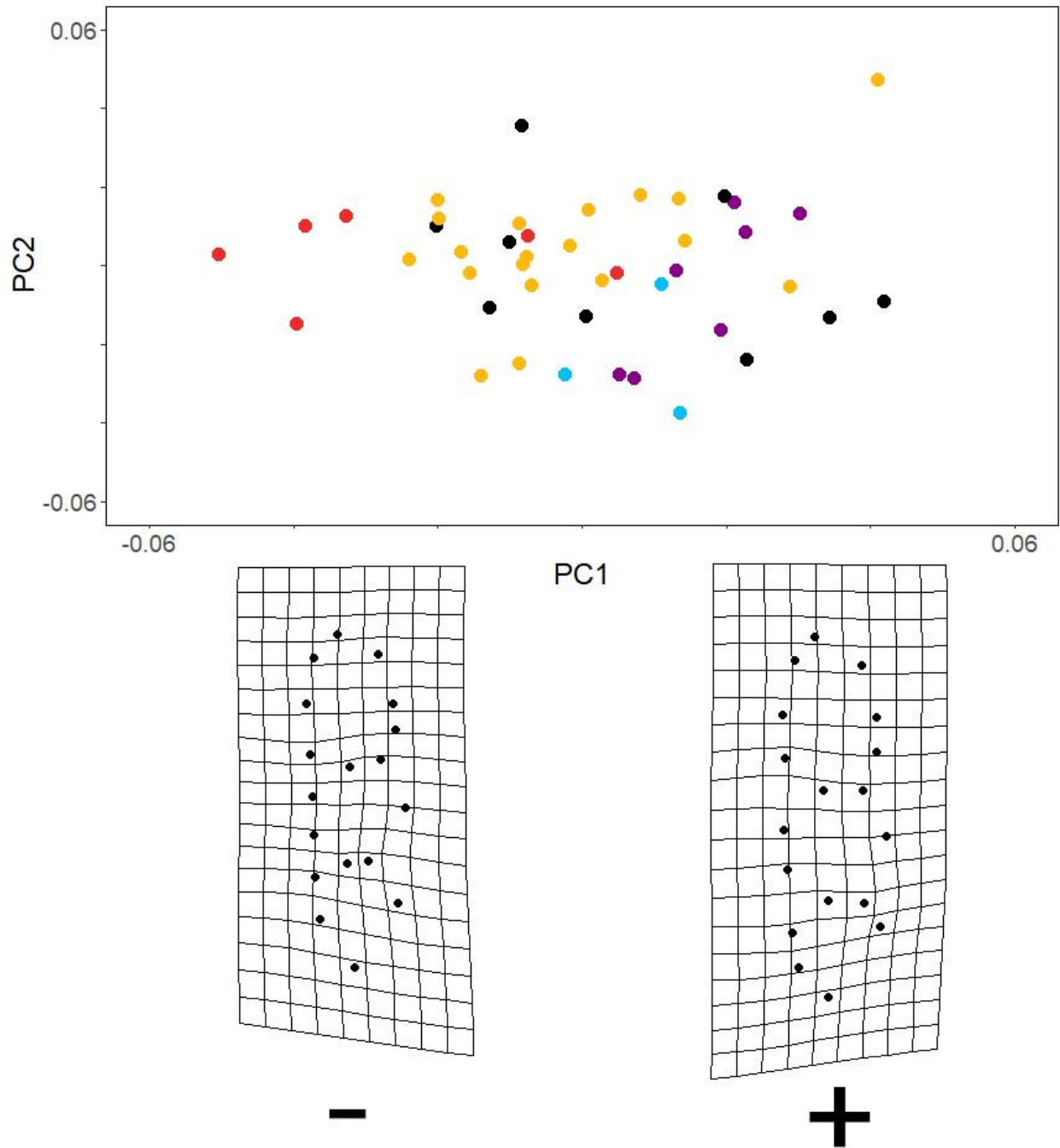
Figure 13A. Plot of PC1 and PC2 showing the different wear stages in *Paulamys naso* (red = stage 1; yellow = stage 2; black = stage 3; purple = stage 4; blue = stage 5). ([back to text](#))
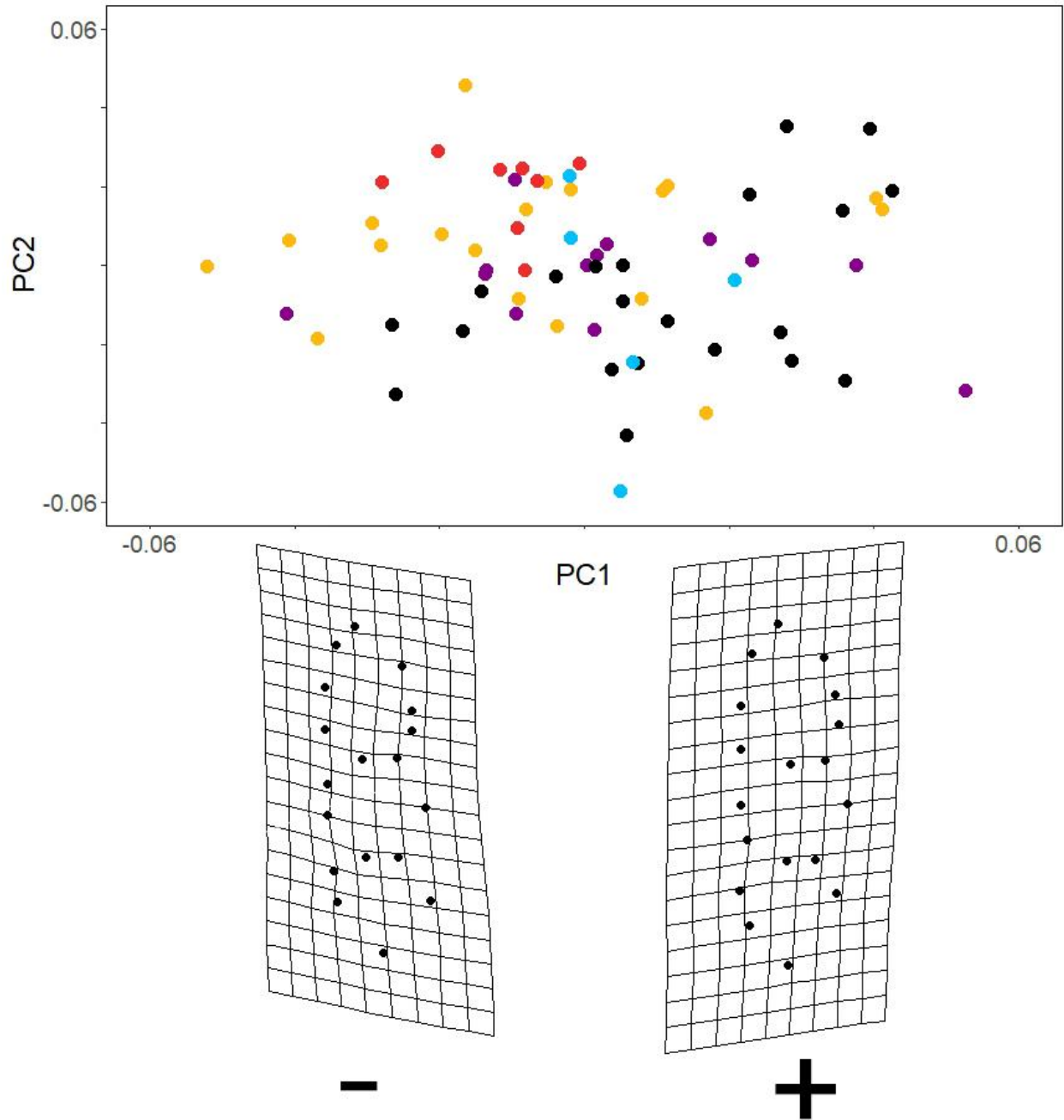
Figure 13B. Plot of PC1 and PC2 showing the different wear stages in *Komodomys rintjanus* (red = stage 1; yellow = stage 2; black = stage 3; purple = stage 4; blue = stage 5). (back to text)
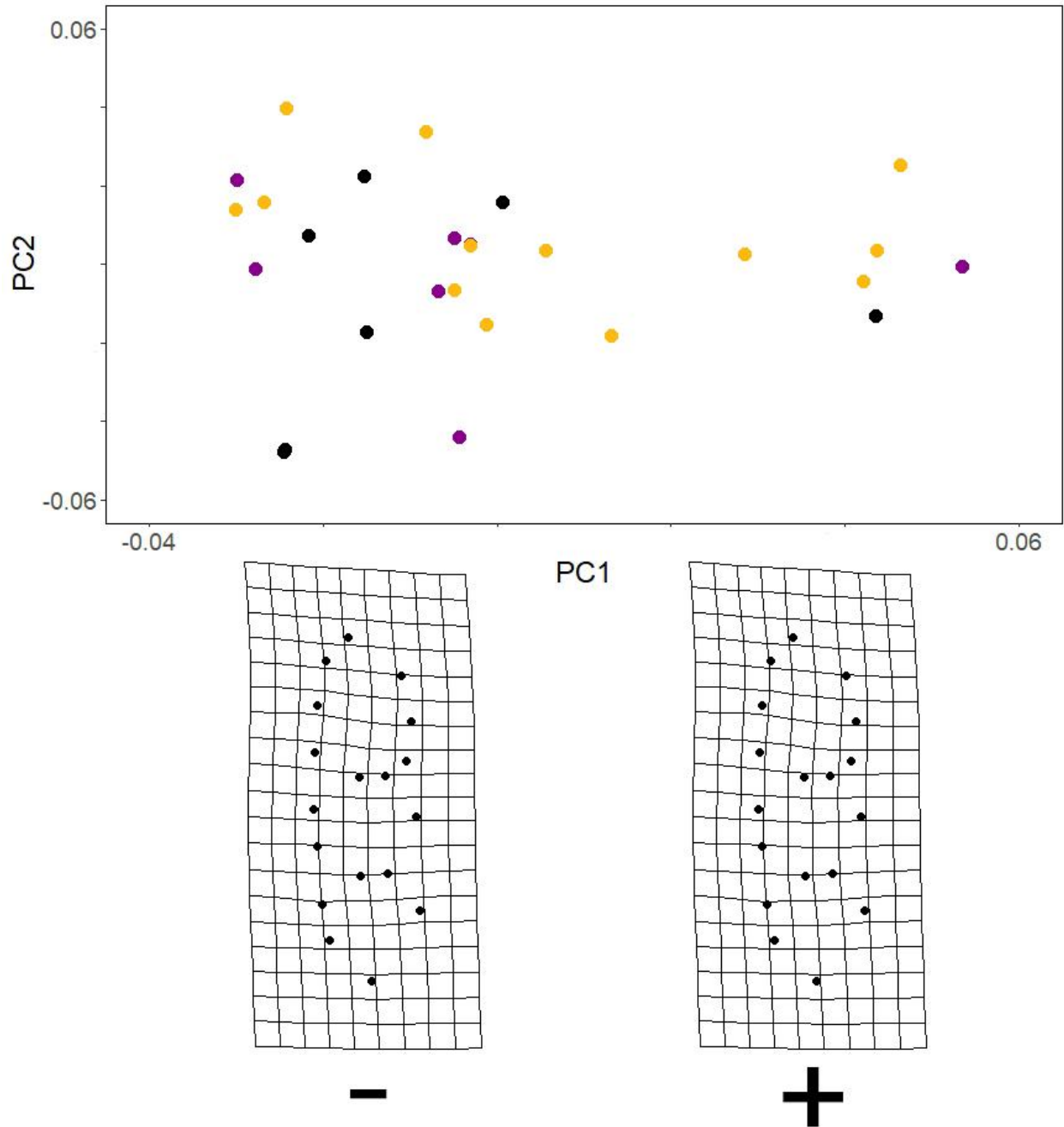
Figure 14. Plot of PC1 and PC2 showing the different wear stages in *Papagomys armandvillei* (yellow = stage 2; black = stage 3; purple = stage 4). ([back to text](#))

Endnotes

[1] Biologically homologous landmarks refer to landmarks that have the same relative position on a biological structure (i.e., a landmark on the exact same point on the tooth regardless of species) (Zelditch et al., 2004).

[2] Centroid size is the sum of the squared distances from each landmark to the centroid of a specimen (Cooke and Terhune, 2015).

[3] Endemic species are those that are native to a particular area (i.e., *Papagomys armandvillei* is native to Flores and found nowhere else) (Wood, 2011).

[4] Holotype refers to a single specimen which a new specimen is based upon and described in the original publication (International Commission on Zoological Nomenclature, 1999).

[5] Congener refers to species who are members of the same genus (i.e., *Papagomys armandvillei* and *Papagomys theodorverhoeveni*) (Park, 2017).

References

Adobe, 2018. Adobe Photoshop. Adobe, USA.

Adams, D.C., Rohlf, F.J., Slice, D.E., 2004. Geometric morphometrics: Ten years of progress following the 'revolution.' Italian Journal of Zoology 71, 5–16.

Adams, D.C., Rohlf, F.J., Slice, D.E., 2013. A field comes of age: Geometric morphometrics in the 21st century. Hystrix 24, 7–14.

Adams, D.C., Collyer, M.L., Kaliontzopoulou, A. 2019. Geomorph: Software for geometric morphometric analyses. R package version 3.1.3. https://cran.r-project.org/package=geomorph

Bailey, S.E., 2004. A morphometric analysis of maxillary molar crowns of Middle-Late Pleistocene hominins. Journal of Human Evolution 47, 183–198.

Brown, P., Maeda, T., 2009. Liang Bua *Homo floresiensis* mandibles and mandibular teeth: A contribution to the comparative morphology of a new hominin species. Journal of Human Evolution 57, 571–596.

Brown, P., Sutikna, T., Morwood, M.J., Soejono, R.P., Jatmiko, Wahyu Saptomo, E., Rokus Awe Due, 2004. A new small-bodied hominin from the Late Pleistocene of Flores, Indonesia. Nature 431, 1055–1061.

Buchtová, M., Stembírek, J., Glocová, K., Matalová, E., Tucker, A.S., 2012. Early regression of the dental lamina underlies the development of diphyodont dentitions. Journal of Dental Research 91, 491–498.

Calede, J., Hopkins, S., 2012. Intraspecific versus interspecific variation in Miocene Great Basin mylagaulids: Implications for systematics and evolutionary history. Zoological Journal of the Linnean Society 164, 427–450.

Calede, J.J.M., Glusman, J.W., 2017. Geometric morphometric analyses of worn cheek teeth help identify extant and extinct gophers (Rodentia, Geomyidae). Palaeontology 60, 281–307.

Cooke, S.B., Terhune, C.E., 2015. Form, function, and geometric morphometrics. The Anatomical Record 298, 5–28.

Cucchi, T., Hulme-Beaman, A., Yuan, J., Dobney, K., 2011. Early Neolithic pig domestication at Jiahu, Henan Province, China: Clues from molar shape analyses using geometric morphometric approaches. Journal of Archaeological Science 38, 11–22.

Delgado, M.N., Gamarra, B., Nadal, J., Mercadal, O., Olesti, O., Guàrdia, J., Pérez-Pérez, A., Galbany, J., 2014. Dental shape variability in cercopithecoid primates: A model for the taxonomic attribution of macaques from Roman archaeological contexts. Folia Primatologica 85, 361–378.

Diekwisch, T.G.H., Berman, B.J., Anderton, X., Gurinsky, B., Ortega, A.J., Satchell, P.G., Williams, M., Arumugham, C., Luan, X., Mcintosh, J.E., Yamane, A., Carlson, D.S., Sire, J.-Y., Shuler, C.F., 2002. Membranes, minerals, and proteins of developing vertebrate enamel. Microscopy Research and Technique 59, 373–395.

Feranec, R.S., Barnosky, A.D., Quang, C.N., 2005. New populations and biogeographic patterns of the geomyid rodents *Lignimus* and *Mojavemys* from the Barstovian of western Montana. Journal of Vertebrate Paleontology 25, 962–975.

Gómez-Robles, A., Martinón-Torres, M., Bermúdez de Castro, J.M., Margvelashvili, A., Bastir, M., Arsuaga, J.L., Pérez-Pérez, A., Estebaranz, F., Martínez, L.M., 2007. A geometric morphometric analysis of hominin upper first molar shape. Journal of Human Evolution 53, 272–285.

Gómez-Robles, A., Martinón-Torres, M., Bermúdez de Castro, J.M., Prado, L., Sarmiento, S., Arsuaga, J.L., 2008. Geometric morphometric analysis of the crown morphology of the lower first premolar of hominins, with special attention to Pleistocene *Homo*. Journal of Human Evolution 55, 627–638.

Gómez-Robles, A., Martinón-Torres, M., Bermúdez de Castro, J.M., Prado-Simón, L., Arsuaga, J.L., 2011. A geometric morphometric analysis of hominin upper premolars. Shape variation and morphological integration. Journal of Human Evolution 61, 688–702.

Gómez-Robles, A., Bermúdez de Castro, J.M., Martinón-Torres, M., Prado-Simón, L., Arsuaga, J.L., 2015. A geometric morphometric analysis of hominin lower molars: Evolutionary implications and overview of postcanine dental variation. Journal of Human Evolution 82, 34–50.

Grine, F.E., Jacobs, R.L., Reed, K.E., Plavcan, J.M., 2012. The enigmatic molar from Gondolin, South Africa: Implications for *Paranthropus* paleobiology. Journal of Human Evolution 63, 597–609.

Hillson, S., 1996. Dental anthropology. Cambridge University Press, Cambridge.

Hillson, S., 2005. Teeth, 2nd ed. Cambridge University Press, Cambridge.

Hooijer, D.A., 1957. Three new giant prehistoric rats from Flores, Lesser Sunda Islands. Zoologische Mededelingen 35, 299–314.

Hulme-Beaman, A., 2014. Exploring the human-mediated dispersal of commensal small mammals using dental morphology: *Rattus exulans* and *Rattus rattus* (Dissertation). University of Aberdeen.

Hulme-Beaman, A., Claude, J., Chaval, Y., Evin, A., Morand, S., Vigne, J.D., Dobney, K., Cucchi, T., 2018a. Dental shape variation and phylogenetic signal in the Rattini tribe species of mainland Southeast Asia. Journal of Mammalian Evolution 26, 435–446

Hulme-Beaman, A., Cucchi, T., Evin, A., Searle, J.B., Dobney, K., 2018b. Exploring *Rattus praetor* (Rodentia, Muridae) as a possible species complex using geometric morphometrics on dental morphology. Mammalian Biology 92, 62–67.

International Commission on Zoological Nomenclature, 1999. International code of zoological nomenclature, 4th ed. International Trust for Zoological Nomenclature.

Kaifu, Y., Kono, R.T., Sutikna, T., Wahyu Saptomo, E., Jatmiko, Rokus Due Awe, 2015. Unique dental morphology of *Homo floresiensis* and its evolutionary implications. PLoS ONE 10, e0141614.

Kendall, D.G., 1977. The diffusion of shape. Advances in Applied Probability 9, 428–430.

Kitchener, D.J., How, R.A., Maharadatunkamsi, 1991a. A new species of *Rattus* from the mountains of West Flores, Indonesia. Records of the Western Australian Museum 15, 611–626.

Kitchener, D.J., How, R.A., Maharadatunkamsi, 1991b. *Paulamys* sp. cf. *P. naso* (Musser, 1981) (Rodentia: Muridae) from Flores Island, Nusa Tenggara, Indonesia: Description from a modern specimen and a consideration of its phylogenetic affinities. Records of the Western Australian Museum 15, 171–189.

Klingenberg, C.P., 2016. Size, shape, and form: Concepts of allometry in geometric morphometrics. Development Genes and Evolution 226, 113–137.

Locatelli, E., Rokus Awe Due, van den Bergh, G.D., van den Hoek Ostende, L.W., 2012. Pleistocene survivors and Holocene extinctions: The giant rats from Liang Bua (Flores, Indonesia). Quaternary International 281, 47–57.

Locatelli, E., Rokus Awe Due, Jatmiko, van den Hoek Ostende, L.W., 2015. Middle-sized murids from Liang Bua (Flores, Indonesia): Insular endemics, human introductions and palaeoenvironment. Palaeobiodiversity and Palaeoenvironments 95, 497–512.

Macdonald, D.A., Royal, K., Buchanan, B., 2020. Evaluating the effects of parallax in archaeological geometric morphometric analyses. Archaeological and Anthropological Sciences 12, 149.

Martinón-Torres, M., Bermúdez de Castro, J.M., Gómez-Robles, A., Margvelashvili, A., Prado, L., Lordkipanidze, D., Vekua, A., 2008. Dental remains from Dmanisi (Republic of Georgia): Morphological analysis and comparative study. Journal of Human Evolution 55, 249–273.

McGuire, J.L., 2011. Identifying California *Microtus* species using geometric morphometrics documents Quaternary geographic range contractions. Journal of Mammalogy 92, 1383–1394.

Misonne, X., 1969. African and Indo-Australian Muridae: Evolutionary trends. Musée royal de l'Afrique centrale, Tervuren.

Musser, G.G., Boeadi, 1980. A new genus of murid rodent from the Komodo Islands in Nusatenggara, Indonesia. Journal of Mammalogy 61, 395–413.

Musser, G.G., 1981. The giant rat of Flores and its relatives east of Borneo and Bali. Bulletin of the American Museum of Natural History 169, 67–176.

Musser, G.G., van de Weerd, A., Strausser, E., 1986. *Paulamys*, a replacement name for Floresomys, Musser, 1981 (Muridae), and new material of that taxon from Flores, Indonesia. American Museum Novitates 2850, 1–10.

Nozaki, S., Amano, H., Oishi, M., Ogihara, N., 2021. Morphological differences in the calcaneus among extant great apes investigated by three-dimensional geometric morphometrics. Scientific Reports 11, 20889.

Park, C., Allaby, M., 2017. A dictionary of environment and conservation, A Dictionary of Environment and Conservation. Oxford University Press.

Purger, J.J., Szép, D., 2022. An attempt to determine the size of the Common Barn-owl's (*Tyto alba*) hunting area based on its prey composition. Avian Biology Research. 15, 41–46.

R Core Team, 2019. R: A language and environment for statistical computing. R Foundation for Statistical Computing, Vienna, Austria. URL: http://www.R-project.org/.

Rohlf, F.J., 1999. Shape statistics: Procrustes superimpositions and tangent spaces. Journal of Classification 16, 197–223.

Rohlf, F.J., 2018. *tpsDIG* (version 2.31). Stony Brook University. https://sbmorphometrics.org/

Rohlf, F.J., 2021. *tpsUTIL32* (version 1.81). Stony Brook University. https://sbmorphometrics.org/

Slice, D.E., 2005. Modern Morphometrics. In: Slice, D.E. (Ed.), Modern morphometrics in physical anthropology, developments in primatology: Progress and prospects. Springer US, Boston, MA, pp. 1–45.

Skinner, M.M., Gunz, P., Wood, B.A., Hublin, J.-J., 2008. Enamel-dentine junction (EDJ) morphology distinguishes the lower molars of *Australopithecus africanus* and *Paranthropus robustus*. Journal of Human Evolution 55, 979–988.

Sody, H.J.V., 1941. On a collection of rats from the Indo-Malayan and Indo-Australian regions. Treubia 18, 255–325.

Sutikna, T., Tocheri, M.W., Morwood, M.J., Wahyu Saptomo, E., Jatmiko, Rokus Due Awe, Wasisto, S., Westaway, K.E., Aubert, M., Li, B., Zhao, J., Storey, M., Alloway, B.V., Morley, M.W., Meijer, H.J.M., van den Bergh, G.D., Grun, R., Dosseto, A., Brumm, A.,

Jungers, W.L., Roberts, R.G., 2016. Revised stratigraphy and chronology for *Homo floresiensis* at Liang Bua in Indonesia. Nature 366–369.

Sutikna, T., Tocheri, M.W., Faith, J.T., Jatmiko, Rokus Due Awe, Meijer, H.J.M., Wahyu Saptomo, E., Roberts, R.G., 2018. The spatio-temporal distribution of archaeological and faunal finds at Liang Bua (Flores, Indonesia) in light of the revised chronology for *Homo floresiensis*. Journal of Human Evolution 124, 52–74.

Swindler, D.R., 2002. Primate Dentition: An introduction to the teeth of non-human primates (Cambridge Studies in Biological and Evolutionary Anthropology). Cambridge University Press, Cambridge.

Thomson, V., Aplin, K.P., Cooper, A., Hisheh, S., Suzuki, H., Maryanto, I., Yap, G., Donnellan, S.C., 2014. Molecular genetic evidence for the place of origin of the Pacific rat, *Rattus exulans*. PLoS ONE 9, e91356–e91356.

Ungar, P.S., 2014. Teeth: A very short introduction. Oxford University Press.

van den Bergh, G.D., Meijer, H.J.M., Rokhus Due Awe, Morwood, M.J., Szabó, K., van den Hoek Ostende, L.W., Sutikna, T., Saptomo, E.W., Piper, P.J., Dobney, K.M., 2009. The Liang Bua faunal remains: A 95 k.yr. sequence from Flores, East Indonesia. Journal of Human Evolution 57, 527–537.

Veatch, E.G., 2014. Morphological analysis of the humerus and calcaneus of endemic rats from Liang Bua, Flores, Indonesia (Thesis). The George Washington University, Washington.

Veatch, E.G., Tocheri, M.W., Sutikna, T., McGrath, K., Wahyu Saptomo, E., Jatmiko, Helgen, K.M., 2019. Temporal shifts in the distribution of murine rodent body size classes at Liang Bua (Flores, Indonesia) reveal new insights into the paleoecology of *Homo floresiensis* and associated fauna. Journal of Human Evolution 130, 45–60.

Veatch, E.G., 2021. The Zooarchaeology and Taphonomy of Small Mammal Remains at Liang Bua, Flores, Indonesia (Dissertation). Emory University, Atlanta.

Wood, B.A., Abbott, S.A., 1983. Analysis of the dental morphology of Plio-pleistocene hominids. I. Mandibular molars: crown area measurements and morphological traits. Journal of Anatomy 136, 197–219.

Wood, B.A., Abbott, S.A., Graham, S.H., 1983. Analysis of the dental morphology of Plio-Pleistocene hominids. II. Mandibular molars-study of cusp areas, fissure pattern and cross sectional shape of the crown. Journal of Anatomy 137, 287–314.

Wood, B. (Ed.), 2011. Wiley-Blackwell encyclopedia of human evolution. John Wiley & Sons, Incorporated, Somerset, United Kingdom.

Wyatt, M.R., Hopkins, S.S.B., Davis, E.B., 2021. Using 2D dental geometric morphometrics to identify modern *Perognathus* and *Chaetodipus* specimens (Rodentia, Heteromyidae). Journal of Mammalogy. 102, 1087–1100.

Zelditch, M.L., Swiderski, D.L., Sheets, H. David, Fink, W.L., 2004. Geometric Morphometrics for Biologists, 1st ed. Academic Press.

Zelditch, M.L., Swiderski, D.L., Sheets, H.D., 2012. Geometric Morphometrics for Biologists: A Primer, 2nd ed. Academic Press, Amsterdam.

Appendix: Shape theory and generalized Procrustes analysis

After landmark data are read in using x, y cartesian coordinates, all non-shape related information must be removed. This is done using a generalized Procrustes analysis (GPA) on all specimens included in the analysis. The GPA is done so that only shape-related information remains and all information about size, position, and rotation is removed (Figure 1) (Zelditch et al., 2004, 2012). To understand how this works, it is first important to understand shape information. Kendall (1977) defines shape as all of the geometric information that is left once size, position, and rotational information is separated and removed from an object. Therefore, to truly assess shape (as is desired in both 2D and 3D geometric morphometrics), all non-shape-related information must be removed. All of this information can be removed without altering the shape by translating, rotating, and scaling the object (Zelditch et al., 2004, 2012).

Figure 1. A visual depiction of the stages of the GPA. Step 1 indicates two triangles (A and B) in their original form. Step 2 shows two triangles that have now been centred upon each other. In step 3, the triangles have been scaled to the same size. Finally, in step 4, the triangles are rotated to minimize the distance between. Note that shape is not altered between stage 1 and 4. (Modified from Zelditch et al., 2012)
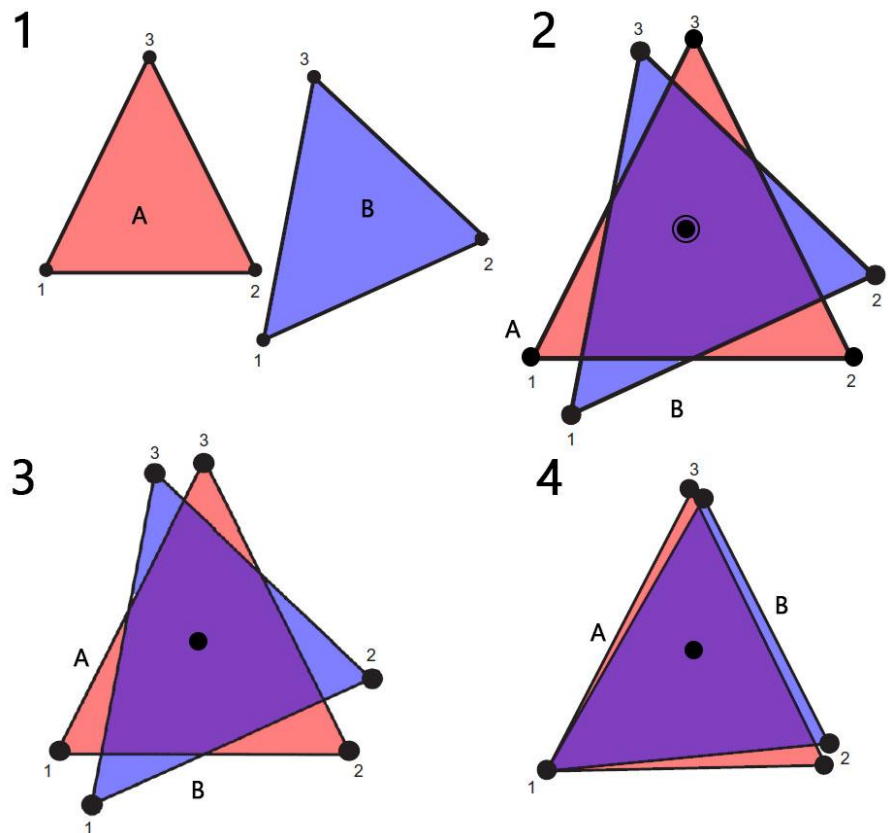
To better understand the GPA process, it is first necessary to understand how the many shapes in an analysis exist in their natural state and how they are transformed. Typically, positional information is removed followed by size and then rotational information (Rohlf, 1999). While the order of removing position and size information is not of utmost importance, information relating to rotation must be removed last (Rohlf, 1999; Zelditch et al., 2004, 2012). Since the GPA is best visualized as a series of steps that must be followed, it is described below based on Zelditch et al. (2004, 2012).

1. **Removing Position**

    To remove positional information, the objects must all be centred upon each other. This is done by calculating the centroid of each shape and lining up the centroids for all objects. Since translation does not affect shape, moving the object left or right and up and down to line up centroids does not change the shape and is justified. Once this positional information is removed, the objects can be thought of as partly superimposed since they now share a common centroid point. Additionally, it is important to note that all objects can have different rotations at this stage of the GPA, this rotational information is irrelevant to removing positional information.

2. **Removing Size**

    To remove size, the centroid of an object is used to calculate centroid size. Since centroid size is not affected by the position of an object, it is ideal for use in geometric morphometrics. Centroid size is calculated as the sum of the square root of distances between each landmark and the centroid. To scale all objects to

the same size, centroid size is set to 1. This step in setting the centroid size to 1

removes size from the equation.

3. **Removing Rotation**

Once positional and size information are removed, the objects are now

thought to be in a pre-shape space. This pre-shape space is a hypersphere in which

every object has a point (i.e., every specimen in an analysis will have its own

point in a pre-shape space) and only rotational information is left to be removed.

It is important to note that objects in pre-shape space can only exist along the

outer surface of the sphere and cannot exist within the sphere as centroid size has

been set to 1, the radius of a sphere. Although each object can be thought of as

having a distinct location in pre-shape space, each object exists along what is

called a fibre. This fibre is a circular arc on which every reachable rotation of an

object is located (Figure 2). Although each object has a fibre along which there

are various rotations, there will be a point at which the distance between objects is

minimized. In a sample with only two specimens, this is easy to visualize as there

is no reference shape required to minimize the difference between; however, in a

sample composed of many objects, there is an additional reference shape in the

shape space. This reference shape is the mathematically defined mean shape of all

objects in a sample which is calculated by averaging the corresponding

homologous landmarks of each object. This is to say that the reference shape does

not represent any single object in a sample but is a new shape that is created and

one that will minimize distortion in further steps.

This mathematically defined mean reference shape also exists within the pre-shape space and has a fibre like all other objects. As such, there are also rotations of this object along its fibre. However, rather than minimizing the distance between two objects, to reach partial procrustes superimpositions, all objects in the pre-shape space will be rotated to minimize the distance between them and the reference shape. When the two objects are aligned to minimize the distance between them, an arc is drawn between them. This arc is known as the Procrustes distance; however, this arc is not the shortest distance between them (Figure 2). Instead, a chord is drawn between the two objects which is the shortest distance possible known as the partial Procrustes distance. Once all objects are rotated to minimize the distance between them and the reference shape, rotational information is removed to the partial Procrustes distances and they can be moved out of a pre-shape space and into a shape space. However, although rotational information is removed, the distance between objects is still not fully minimized as they can be moved into the sphere.
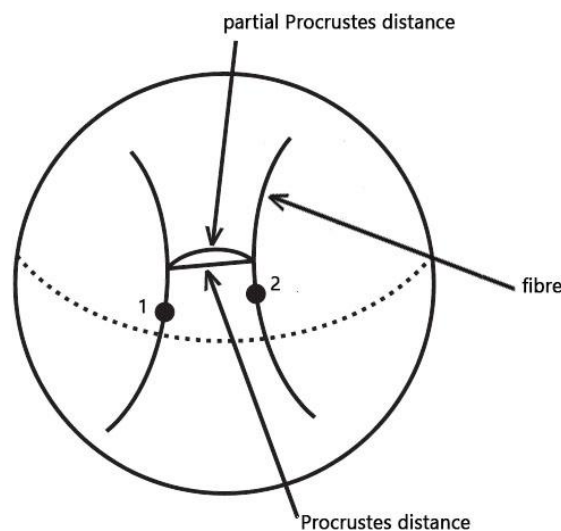

Figure 2. Visualization of pre-shape space containing two fibres (circular arches 1 & 2) with both the partial Procrustes and Procrustes distances indicated (modified from Zelditch et al., 2012).

4. Kendall's Shape Space

Once out of the pre-shape space, objects can be thought of as moving into a new sphere known as Kendall's shape space. Like the pre-shape space, Kendall's shape space is also a hypersphere; however, it differs in that objects can be moved *into* the sphere rather than just being moved along the outer surface of the sphere. To do this, the centroid size has to be changed from 1 to the value of cos(*p*). In doing so, the object is moved *into* the sphere and a new, smaller, sphere is created connecting the reference shape at the pole and the object being moved into the sphere. Once the object is moved into the sphere, the distance between the object and reference shape has been fully minimized. This distance is now known as the full Procrustes distance.
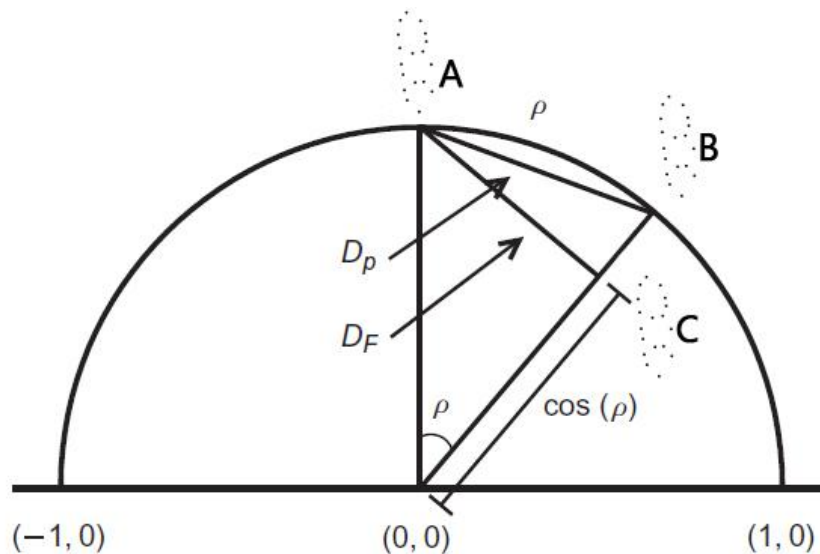

Figure 3. Visual depiction of Kendall's shape space showing the Procrustes distance (*p*), partial Procrustes distance (D_p) and full Procrustes distance (D_F) in addition to the steps to get to fully minimize Procruestes distances (A) the initial position of an object; (B) object rotated to partial Procrustes distance; (C) object rotated to full Procrustes distance (modified from Zelditch et al., 2012).

With all objects in Kendall's shape space with the Procrustes distances fully minimized to the full Procrustes distance, non-shape data related information has been fully removed. Objects can now be projected onto the tangent plane. This can be visualized as a plane placed on the pole of the outer sphere of Kendall's shape space known as the tangent plane. Along this plane, the reference shape positioned at the pole of Kendall's shape space must have the coordinates of (0,0). While this reference shape will not appear in any projection, its orientation on the place is nonetheless important. From here, all other objects in Kendall's shape space can be projected orthogonally or stereoscopically with statistically negligible differences if the reference shape is the mathematical mean.

Completing all of these steps will complete the GPA and data are then analyzed using ordination methods such as a PCA (Zelditch et al., 2004, 2012). The information remaining after the completion of the GPA includes only information relating to shape; however, the data are still hyperdimensional as the pre-shape space and Kendall's shape space exist as hyperspheres (Zelditch et al., 2004, 2012). Since a PCA requires no *a priori* assumptions about group membership, it is used to emphasize variation between individuals rather than between groups. However, the non-linear Procrustes data produced by the GPA violates key theory of the PCA, which assumes a linear Euclidean space (Slice, 2005). Although the original Procrustes data violate this assumption, these data can be projected to a linear tangent space to both preserve the distance between specimens and create linear data (Slice, 2005). To do this, the Procrustes shape data produced by the GPA are projected into an approximation of a linear space using the tangent plane from Kendall's shape space (Slice, 2005).

Although there are multiple types of projections that can be used, it is thought that an orthogonal projection best preserves the distances between specimens (Slice, 2005). However, due to the small amount of variation that is likely to be exhibited in any biological sample, other projections are unlikely to produce statistically different results (Slice, 2005; Zelditch et al., 2012). In essence, the tangent plane is able to rotate and dissect any part of the shape space so long as the reference shape remains at (0,0) and create a projection that maximizes the difference between objects (Zelditch et al., 2012). Objects are projected onto the tangent plane into a linear Euclidean space from the shape space which creates linear data that does not significantly differ from the original shape data that can be manipulated and analyzed (Zelditch et al., 2012). While there are alternative methods of deriving shape variables from both partial and full Procrustes superimposed data, this method uses the tangent plane as the principal component axis (Rohlf, 1999). In this case, the tangent plane is oriented through the shape space (with the reference shape at (0,0) in a way that maximizes the differences between objects in the shape space (Rohlf, 1999). The objects in the shape space are then orthogonally projected into the tangent space across the tangent plane/principal component axis to produce coordinates also known as Kendall tangent space coordinates (Rohlf, 1999). This projection forms a visualization of principal component 1 (PC1). From there, the second principal component (PC2) (which represents the second most variation) is orthogonal to PC1.

The GPA, the projection, and interpretation of shape date are complex processes that are firmly grounded in mathematical principles. However, these processes are required to turn landmark-based data into something that can be more easily interpreted and understood. Since the GPA produces strictly shape data, it is difficult to interpret without any further analysis.

Figure 4 shows an example of shape data that is produced using the GPA; however, it is clear that without a subsequent PCA, it is difficult to discern how shape changes between the specimens. Together, with the GPA and PCA, shape data are analyzed to produce meaningful biological information about a sample.
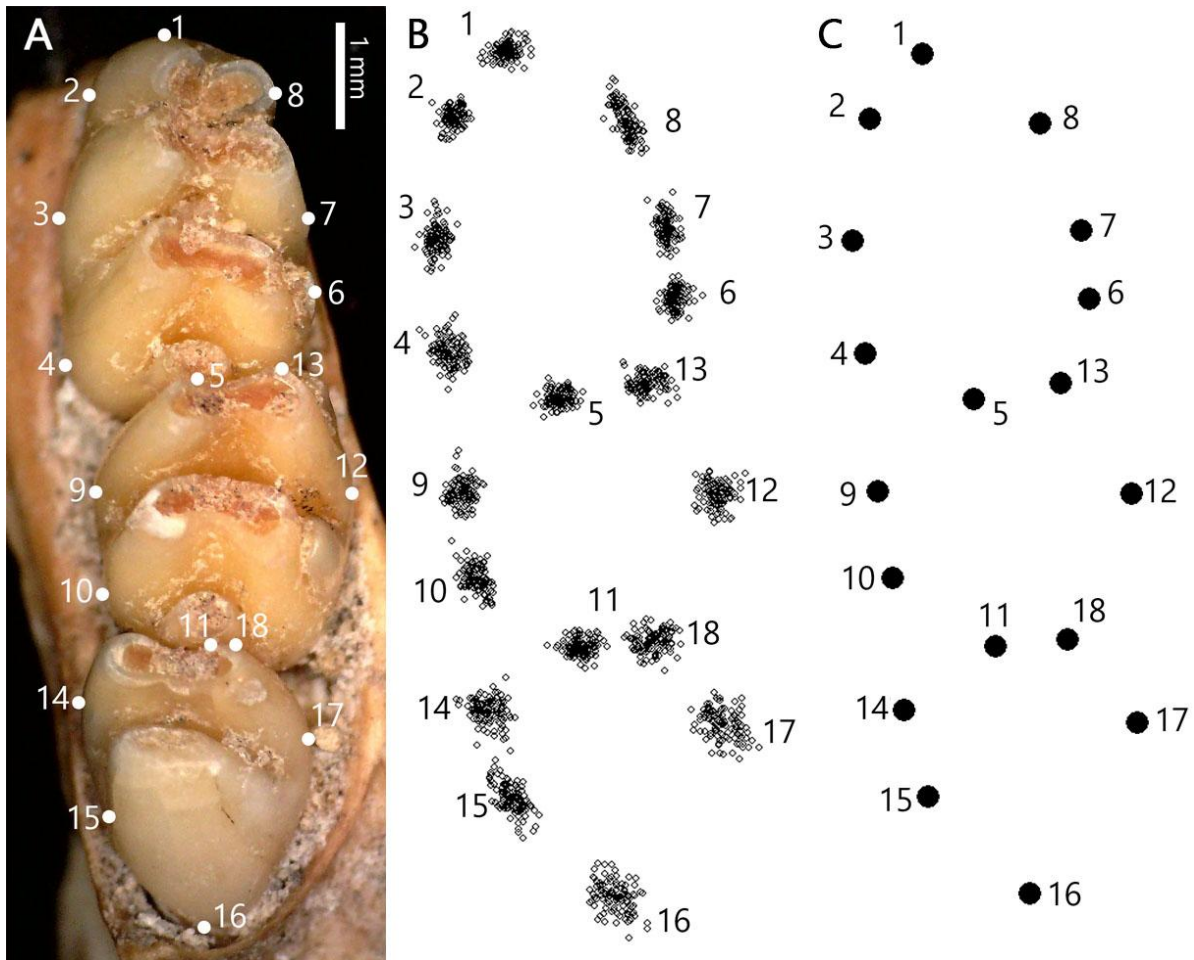

Figure 4. An example of shape data produced by the GPA. Original landmark data (A) are shown on a single toothrow. Using 112 specimens, shape data are produced (B) with a cluster for each landmark. Using the data from all 112 specimens, a reference shape (C) is created.